POST-HARVEST QUALITY EVALUATION BY PULSED THERMOGRAPHIC INSPECTION

by

JESSE KUZY

(Under the Direction of Changying “Charlie” Li)

ABSTRACT

Pulsed thermographic inspection is native to the domain of fault inspection in rigid bodies such as polymer and metal plates. Recent research has shown that it also has some utility for agricultural applications, such as the detection of foreign bodies in bulk harvested goods. For the problems of cotton foreign matter detection and blueberry bruise detection, a variety of sensing modalities have been applied, but to date no research has been conducted into the use of thermal imaging to accomplish these tasks. We perform pulsed thermographic inspection of cotton foreign matter and cotton lint, extract appropriate features, and demonstrate the ability to discriminate between classes on the basis of these features. Similarly, we examine bruised and healthy blueberries and show that they can be differentiated by pulsed thermographic inspection.

INDEX WORDS: Thermal Imaging, Pulse-phase Thermography, Post-harvest Quality Inspection, Cotton Foreign Matter, Blueberry Bruise Detection

POST-HARVEST QUALITY EVALUATION BY PULSED THERMOGRAPHIC INSPECTION

by

JESSE KUZY

B.S. Biomedical Engineering, Georgia Institute of Technology, 2011

A Thesis Submitted to the Graduate Faculty of The University of Georgia in Partial Fulfillment of the Requirements for the Degree

MASTER OF SCIENCE

ATHENS, GEORGIA

2017

POST-HARVEST QUALITY EVALUATION BY PULSED THERMOGRAPHIC INSPECTION

by

JESSE KUZY

Major Professor:	Changying “Charlie” Li
Committee:	Khaled Rasheed
	Don Potter

Electronic Version Approved:

Suzanne Barbour
Dean of the Graduate School
The University of Georgia
August 2017

DEDICATION

To the workers of the world. A new day is dawning.

ACKNOWLEDGEMENTS

I would like to express my gratitude to my major professor and PI, Changying Li, for his support and assistance throughout the course of my studies. I would also like to extend my thanks to the members of my thesis committee, Dr. Potter and Dr. Rasheed, for their time, service, and patience.

TABLE OF CONTENTS

Page

LIST OF TABLES

Page

LIST OF FIGURES

Page

CHAPTER 1

INTRODUCTION AND LITERATURE REVIEW

1.1 BACKGROUND AND MOTIVATION

This study seeks to explore the possibility of accomplishing two post-harvest quality evaluation tasks using pulsed thermographic inspection techniques. With the popularization of uncooled microbolometer thermal cameras, these devices have become more portable and less expensive, and accordingly, more common in research settings. This has generated increased interest in the potential for this sensing modality to improve results or solve difficult issues in the domain of post-harvest quality evaluation. The specific tasks attempted in this study are cotton trash detection and identification, and blueberry bruise detection.

1.1.1 Cotton Trash Detection and Identification

At the time of ginning, harvested cotton lint virtually always contains significant amounts of botanical and synthetic debris. If this foreign matter is permitted to remain in the lint throughout processing and into yarn spinning, the resulting textiles suffer in quality, entailing economic losses for all involved in the processing chain of textile production. High proportions of foreign matter in the cotton lint also creates a variety of considerations for the processors, as the resulting introduction of oil and dust into processing machinery necessitates regular cleaning and careful monitoring of the state of the machinery [1].

The most common foreign matter types are parts of the cotton plant: fragments of leaves, stems, seeds seed coats, hulls, bract, and so on. Also common are foreign fibers such as woven cotton, plastic, and jute, either from wind-blown debris or from baling tarps and twine. Lastly,

various oils and greases may stain the cotton from contact with harvesting and processing machinery [2].

The ginning process removes much of this debris, especially large debris; this is to be expected, since ginning was invented for the express purpose of removing cotton seeds from harvested lint. However, some debris, especially leaves and bract, may simply be broken into ever-smaller pieces, eventually becoming essentially impossible to remove from the lint. This phenomenon is so ubiquitous that the standard cotton classification table contains two axes: one for color and quality of the cotton fibers themselves, and another for the amount of foreign matter present, described by the shorthand "leaf grade, [3]" which reveals the predominance of leaf fragments in foreign matter types observed.

The industry standard device for the evaluation of cotton quality and foreign matter content is the High-Volume Instrument (HVI), which returns metrics including fiber length, uniformity, and strength; micronaire; color; and foreign matter content [3]. Another popular device, the Advanced Fiber Information System (AFIS), returns additional detailed information about the cotton fibers themselves. These techniques are frequently coupled with human inspection, which makes use of published USDA standards to describe the cotton coloration and foreign matter content. Of note is that none of these systems or techniques provide any information about the identity of the foreign matter. All foreign matter is summarized generically as "leaf grade" or "foreign matter content," masking the diversity of foreign matter types present in the cotton lint.

A variety of sensing modalities have been applied to the task of improving the detection rate of foreign matter and providing additional information about the nature of the foreign matter present. These include machine vision with standard RGB images [4,5], Fourier-Transform

Near-Infrared Spectroscopy [6,7], hyperspectral imaging [8,9], fluorescence imaging [10,11], and X-ray microtomography [12,13]. However, to the best of the authors' knowledge, no research groups have published results from attempts to apply thermographic inspection to the task of cotton trash detection.

A somewhat comparable task which was attempted, and performed successfully, by a research group was the detection of foreign bodies present in harvested nuts by Meinlschmidt and Maergner [14], who concluded that the detection of foreign bodies was possible due to differences in the thermal properties of the nuts and foreign bodies. Since cotton and cotton foreign matter also differ in their thermal properties, this provides the basis to motivate exploration of the potential for detecting and identifying cotton foreign matter using thermographic inspection techniques.

1.1.2 Blueberry Bruise Detection

During processing, blueberries must be sorted to remove debris and berries of poor quality. Berries may be underripe, rotten, mechanically damaged, or infested with fungal growths. Many of these defects are detectable by visual inspection, and are accordingly removed by line workers. However, more subtle damages to the tissues are still a concern, as they negatively impact flavor, texture, and shelf life, and increase the rates of rejection by consumers. Berries whose tissues are mechanically damaged in a global fashion, that is, throughout most or all of the berry, can be detected by soft-sorter machines which palpate the berries and reject those which are insufficiently firm. However, this technique relies on direct physical contact between the bruised regions and the actuator of the sorting machine. For berries which are bruised only in small regions, there is some chance that they will pass inspection by the soft-sorter despite having significant regions of tissue damage. Such moderately damaged berries are

best diverted to product streams other than fresh-market sale, such as preserves and baking mixes. The successful detection of blueberry bruises is therefore a significant financial consideration for growers, packers, and distributors.

Researchers have attempted to apply many methods to the evaluation of blueberry quality, including color image analysis [15-17], hyperspectral imaging in the modes of reflectance [18,19], transmittance [20], and interactance [21], and even electronic olfaction [22,23]. Several research groups have applied thermal imaging to the detection of fruit bruises in apples, pears, and citrus fruits [24-28], generally with success, and at times producing information about the depth and severity of bruising. To date, no research group has published findings of studies performed at the intersection of these two strands of research: blueberry bruise detection by thermographic inspection. The successful detection of fruit bruises in other fruit types and the economic importance of bruise detection to the blueberry industry motivate investigation into the applicability of thermal imaging technology to blueberry bruise detection.

1.1.3 Thermographic inspection

The core equation which governs all thermographic inspection techniques is the Stefan-Boltzmann Law, Eq. 1.1:

$$E = \varepsilon \sigma T^4 \tag{3.1}$$

Here E is the total emitted radiation in W/m^2, ε is the emissivity of the object of interest, dimensionless, σ is the Stefan-Boltzman constant in W/m^2K^2, and T is the temperature in Kelvins. Immediately apparent in this equation is the exponent of the temperature term, which indicates that the amount of thermal energy emitted is most highly dependent on the temperature of the emitting object. This is what enables the derivation of the temperature of an object based on the observed emitted radiation. The emissivity is also important, however, and determining

the emissivity of an object is frequently an important experimental task to ensure accurate temperature readings from thermographic data.

Broadly speaking, thermographic techniques can be divided into two families: passive and active. In passive thermographic techniques, objects are observed with no external thermal stimulus applied by the observer. These techniques are suitable for discriminating between objects with different temperatures or emissivities [29], or for the characterization of systems which are thermally dynamic [30]. However, for objects which have the same emissivity, the same resting temperature, and which are in a state of thermal equilibrium, passive thermal techniques will not reveal any differences between the properties of the objects.

For such situations, active thermographic techniques must be applied. In active thermography, an external thermal stimulus is applied to the objects being examined in order to induce thermal disequilibrium. The distribution and redistribution of thermal energy within the object, as indicated by the observed temperatures of the object, are then analyzed to derive information about the material properties of the object. A variety of methods for thermal stimulation can be applied. Varith et. al. used convective heating and cooling treatments to reveal differences between bruised and healthy apple tissues which were not apparent at thermal equilibrium [27]. For rigid bodies, especially for the purpose of detecting small cracks and flaws, ultrasonic stimulation can be applied, causing heat to be generated at flaws were the material rubs against itself [31]. However, the most common type of thermal stimulation is radiative, often with flash lamps [32] or high-powered lamps [25]. Radio waves, microwaves, and other forms of radiative stimulation outside of visible and infrared are infrequently used, as the analysis of the distribution of heating that occurs when such methods are applied is a problem unto itself even for homogeneous materials.

Within radiative methods of active thermography, there are yet more subdivisions of techniques. One technique is lock-in thermography, in which the thermal stimulation applied to the target object is sinusoidally modulated. Over time, the temperature of the target object follows a sinusoidal pattern of the same frequency as the stimulus source, but with a phase offset. Analysis of the magnitude of the phase offset at different portions of the target object may reveal sub-surface flaws and defects [28]. In Xavier Maldague's 1996 paper "Pulse phase infrared thermography," [33] it was demonstrated that this analytical technique is applicable even when the stimulus applied is not sinusoidally modulated, but instead a single thermal pulse. By applying a temporal Fourier transform to the observed thermal response of the target object to the thermal stimulus, the thermal signal can be decomposed into a series of sinusoids of varying frequencies, each of which has an associated phase and amplitude values. By examining the pertinent phase values (the determination of which phase values are of interest being a question of some import) one can not only detect sub-surface defects, but moreover, estimates can be produced of the depth of the defect [34]. Due to Maldague's emphasis on the phase values, which in his evaluation had properties superior to the amplitude values, this analytical technique became known as pulse-phase thermography.

1.2 EXPECTED RESULTS

For the cotton trash task, it is expected that findings will be positive for at least some trash types. The various classes of cotton trash differ significantly in the material properties; a cotton seed has a radically different geometry and material composition than a sample of bract. This should lead to significant differences in the thermal responses of different trash types. Most important, however, is the question of whether it will be possible to distinguish between cotton and the foreign matter samples. Again, it is expected that at least some foreign matter samples

will be distinguishable, owing to their dissimilarity to cotton lint. Others may prove more problematic; twine, for example, is woven strands of plant fiber, and might therefore be expected to show a thermal response similar to cotton lint. Further complicating this task is the highly heterogeneous structure of cotton lint. The lint may form into dense knots and tangles, or may instead be loose and straight; these different spatial configurations may produce different thermal responses, with, for example, knotted lint retaining large quantities of thermal energy where straight, fluffed lint disperses received thermal energy rapidly. This variance in the thermal response of cotton may make it difficult to discriminate well between cotton and all types of foreign matter.

The blueberry bruise detection task also presents significant problems. While bract and a cotton seed may differ radically, a bruised and healthy blueberry differ in significantly more subtle ways. Their geometries and constituent materials are virtually identical. The only differences between the two will be those caused by bruising: ruptured cell walls, compression of tissues, air pockets, and free water content in the intracellular matrix. Whether these differences will result in sufficiently different thermal responses to permit discrimination between bruised and healthy berries is not immediately apparent. Furthermore, variations within treatment groups may obscure any differences between treatments. Variation in the size of berries may be problematic, since a large berry should be expected to heat and cool more slowly than a small berry due to its increased thermal inertia. Different cultivars may have different tissue textures, different skin properties, and so on. Worse still, interaction effects could complicate the data. For example, it may be that one cultivar is more susceptible to bruising than another, and so shows larger variation between treatments. These potential pitfalls will necessitate careful handling of the data and examination of subsets within the data.

CHAPTER 2

A PULSED THERMOGRAPHIC IMAGING SYSTEM FOR DETECTION AND IDENTIFICATION OF COTTON FOREIGN MATTER[1]

[1] Kuzy, J., Li, C., 2016. *Sensors*. *17*(3), 518. Reprinted here with permission of the publisher.

ABSTRACT

Detection of foreign matter in cleaned cotton is instrumental to accurately grading cotton quality, which in turn impacts the marketability of the cotton. Current grading systems return estimates of the amount of foreign matter present, but provide no information about the identity of the contaminants. This paper explores the use of pulsed thermographic analysis to detect and identify cotton foreign matter. The design and implementation of a pulsed thermographic analysis system is described. A sample set of 240 foreign matter and cotton lint samples were collected. Hand-crafted waveform features and frequency-domain features were extracted and analyzed for statistical significance. Classification was performed on these features using linear discriminant analysis and support vector machines. Using waveform features and linear discriminant analysis, detection of cotton foreign matter was performed with 99.58% accuracy; Using either waveform or frequency-domain features, identification was performed with 90.00% accuracy. These results demonstrate that pulsed thermographic imaging analysis produces data which is of significant utility for the detection and identification of cotton foreign matter.

2.1 INTRODUCTION

During harvest and transportation, cotton is contaminated by foreign matter. The most common type foreign matter is botanical matter from the cotton plants: leaf fragments, hulls, stems, seeds, seed coats, and so on; followed by foreign fibers and textiles made of cotton, plastic, and jute; and least common are inorganic debris and oily substances [1]. Prior to ginning, seeds and seed coats are also present. During baling and transportation, cotton may be contaminated with baling twine, fragments of module cover, or grease and oil from machinery. Exogenous debris such as windblown paper and plastic fragments are also occasionally incorporated during harvest. Much of this debris, especially large pieces of debris such as seeds and stems, is removed during

the ginning and cleaning process. Other types of foreign matter may be broken into smaller fragments and not removed; leaf fragments are the most prevalent of these. Following cleaning, cotton is graded according to, among other metrics, its foreign matter content. Cotton containing a high proportion of foreign matter results in defects in textiles, as well as interfering with processing equipment by introducing oil and dust [2]. The detection of cotton foreign matter is therefore a paramount financial consideration for growers, ginners, and textile manufacturers.

The current industry standard device for cotton grading is the High-Volume Instrument (HVI), which measures properties of the cotton including fiber length, uniformity, and strength, micronaire, color, and foreign matter content [3]. This is frequently coupled with human grading, especially for additional analysis of the foreign matter content. It is notable that this system is not capable of determining the type of foreign matter present, nor are human graders tasked with making this determination. USDA standards describe the foreign matter content of cotton batches in terms of "leaf grade." The use of this term implies that foreign matter is comprised primarily of leaves and similar botanical debris. Though this is generally the case, it masks the diversity of foreign matter types encountered in cotton lint. The Advanced Fiber Information System (AFIS), another industrial system, shares this shortcoming [4].

The low cost and ease of implementation of CCD and CMOS color cameras has led many researchers to attempt detection using RGB machine vision. Xu et al. used CCD cameras and Xenon illumination to show a strong correspondence between CCD, HVI, and human grading on estimates of foreign matter content and cotton color measurements [5]. Later studies by Yang et al. combined color and UV illumination for foreign matter detection and achieved a mean detection accuracy of 92.34% using both color and shape features [6,7]. However, white foreign matter was

problematic, and other researchers have pointed out that shape characteristics are not ideal, since mechanical harvesters can produce foreign matter scraps in an endless variety of shapes [8].

Significant research has been devoted to the identification of foreign matter by Fourier-Transform Near-Infrared Spectroscopy (FT-NIR). These techniques use the absorbance spectra of cotton and foreign matter as the basis for discrimination between substances. Fortier et al. have produced a pair of studies using this technique demonstrating 97% accuracy of classification on a set of four foreign matter types (hull, leaf, seed, stem) [9] and 98% accuracy on a set of eight foreign matter types (hull, leaf, seed coat, seed meat, stem, plastic, twine) [10]. The primary weakness of FT-NIR detection techniques is that they are point-based, presenting difficulties for high-volume application; another weakness is the necessity of compiling libraries of the spectral characteristics of the materials of interest, a significant complication [2].

A combination of machine vision methods and FT-NIR methods is hyperspectral imaging, which uses the transmittance or reflectance modes to collect spectra for every visible pixel of a sample. Jiang et al. showed that spectral features derived from this method provide a statistical basis to separate all of 15 foreign matter types except brown leaves and bract [11]. Guo et al. achieved some success in this area, particularly for the detection of foreign fibers, which are a common contaminant in Chinese cotton fields [12]. Using mean NIR spectra collected from a set of 16 foreign matter types and cleaned cotton lint, Zhang et al. achieved an accuracy of classification of 96.5% using LDA classifiers, including 100% accuracy on the cotton lint [13].

Some researchers have taken advantage of the natural fluorescence of cotton foreign matter to perform detection. Gamble and Foulk [14] were able to reliably identify leaves and hull by fluorescence spectroscopy. Mustafic et al. replicated these findings using fluorescence imaging under blue illumination, and additionally demonstrated excellent classification of paper, plastic

module cover, and commercial plastic bag under UV excitation [15]. Using X-ray microtomography, Pai et al. achieved an average classification rate of 96% on a sample set including seed coats, bark, and polypropylene [16]. However, the expense of the instrumentation and the necessity of strict controls on worker exposure to radiation are both obstacles to industrial implementation of this technology.

One imaging modality that has not been applied to the problem of cotton foreign matter detection is thermal imaging. Thermal imaging has been applied to a wide variety of post-harvest quality evaluation tasks, such as detecting mechanical damage and bruising in apples [17]; evaluating the quality of apple wax coatings [18]; detecting soft spots on tomatoes [19]; and detecting insect infestation in wheat kernels [20]. Pulsed and lock-in thermographic techniques have been used to detect apple bruises [21-23], with Varith et al. theorizing that the observed difference in the temperatures of bruised and healthy tissues can be attributed to different thermal diffusivities in the tissues. Specifically, higher thermal diffusivities in bruised tissues create a "thermal window" which allows the rapid flow of heat from the exterior to the interior of the apple, resulting in a lower surface temperature in bruised regions. Meinlschmidt and Maergner (2002) demonstrated that hazelnuts have different thermal properties from typical foreign bodies present in harvested nuts, and developed a thermal imaging system to detect these foreign bodies by heating the nuts and foreign bodies with a flash lamp [24]. Detection was successfully conducted and the researchers concluded that this was possible due to the differing thermal properties of the nuts and foreign bodies [25]. Since it is also the case that cotton and cotton contaminants differ in their thermal properties (although the degree of difference may be minimal for some contaminants), it should be possible to discriminate between cotton and its contaminants using similar techniques. Furthermore, since cotton is dried with hot air in early ginning stages, then

returns to the general processing floor with temperatures nearer to ambient, both cotton and the foreign matter it contains are already exposed to a sharp rise and fall in temperature as part of the ginning process. This may enable use of the technology without any exogenous heat source.

The goal of this paper was to explore the feasibility of using pulsed thermographic imaging technique to detect and classify the cotton foreign matter. Specific objectives were to 1) Design and construct a pulsed thermographic analysis system with imaging acquisition software and data processing pipeline; 2) Extract and evaluate the effectiveness of frequency-domain features and thermal waveform features; and 3) Perform classifications of common cotton contaminants using these features.

2.1.1 Pulse-Phase Thermography

Thermographic analysis is the estimation of a target's temperature based on the magnitude of thermal radiation (infrared radiation) emitted by the target. The relationship between the emitted radiation and the temperature of the observed object is governed by the Stefan-Boltzmann law [26], eq. (1):

$$E = \varepsilon \sigma T^4 \tag{1}$$

E is the total emitted radiation in W/m2, ε is the emissivity of the object, dimensionless, σ is the Stefan-Boltzman constant in W/m2K2, and T is the absolute temperature in °K. Since temperature is the dominating term in the right-hand side of the equation, and since emissivity is a static property for most substances, any observed changes in emitted radiation can be attributed to changes in the temperature of the object.

One method that can reveal additional properties of the target object is active thermography: in active thermographic techniques, an external source of heat is applied the object. The change in the object's temperature over time is then monitored. A specific technique within this family is

pulsed thermography: a radiative heat source is turned on and off at set time intervals, applying a pulse of heat to the object. The redistribution of heat within the object is influenced by a variety of material properties, such as thermal diffusivity, heat capacity, and the geometry of the object. In addition to radiated energy, the object may lose heat from conduction or convection, both of which will also be related to various properties of the material.

Pulse-phase thermography is an analytical technique for pulsed thermographic analysis [27]. In this technique, the changing temperature of each pixel of the observed object is considered as a thermal signal with a temporal dimension, and the Fourier transform is applied to this signal, decomposing it into a sum of sinusoidal components (Figure 2.1). Since the full characterization of the thermal signals of the object pixels is contained in both the amplitude and phase data, both of these values are of interest as potential features for discrimination of samples.

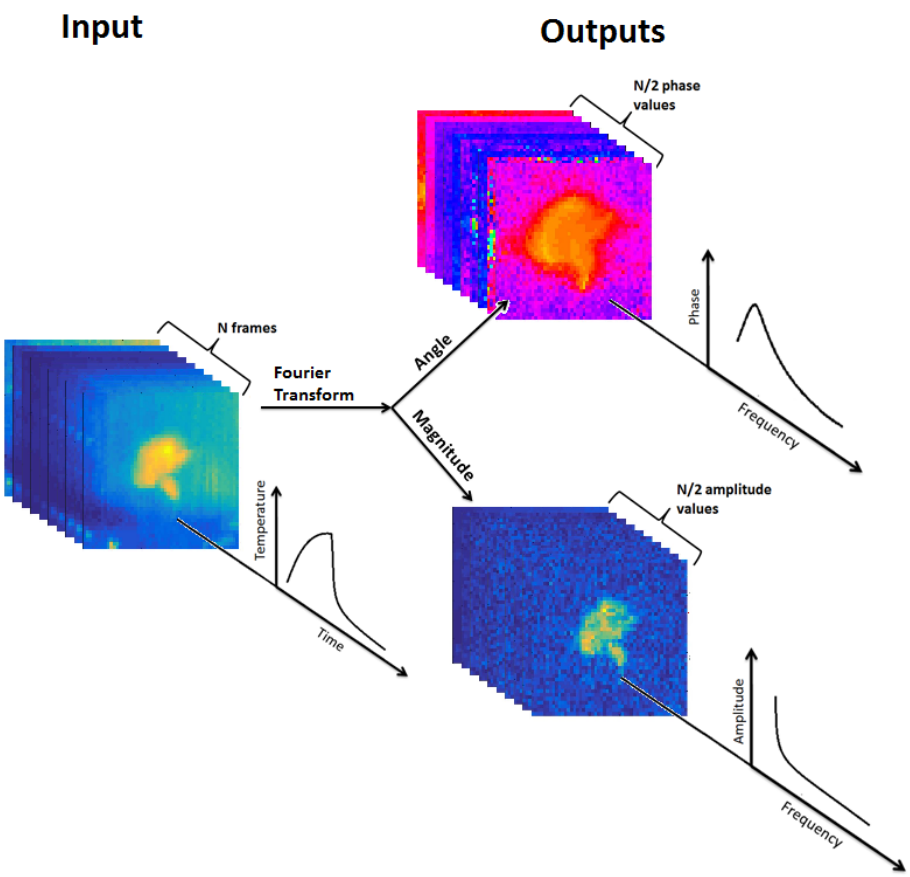

Figure 2.1. Illustration of temporal Fourier transform of cotton foreign matter pulsed thermography videos: Temporal image stack produces phasegram and ampligram image stacks

2.2. MATERIALS AND METHODS

2.2.1. Samples

For this study, eleven types of common cotton contaminants were examined: bark, bract, brown leaves, green leaves, hulls, module cover, paper, seed coats, seeds, stems, and twine (Figure 2.2). Botanical foreign matter samples were extracted from seed cotton samples of four cultivars planted and harvested in 2012: Delta Pine 0912; Delta Pine 1050; PhytoGen 499; and FiberMax 1944. Paper and twine samples were purchased through common consumer channels. Module cover samples were taken from a cotton gin in Tifton, GA. Large scraps were collected and roughly

cut into small squares with side lengths in the range 2-5 mm. For each foreign matter type, 20 samples were analyzed. Additionally, 20 samples of cleaned cotton lint of the aforementioned cultivars were analyzed. In total, 240 samples of cotton and foreign matter were used in this study.

Figure 2.2. Color photographs of foreign matter and cotton lint samples representative of the classes used in this study

2.2.2. Pulsed thermographic imaging system and data acquisition

A pulsed thermography system was constructed to facilitate the performance of pulsed thermographic analysis (Figure 2.3). A general-use laptop (Getac S400, Windows 8.1 Pro 64-bit, Intel Core i5-4210M CPU, 8 Gb RAM) with LabVIEW (National Instruments, Austin, Texas, USA) installed served as the operating terminal. Videos were collected by a FLIR (FLIR Systems, Wilsonville, Oregon, USA) T440 thermal camera mounted on a frame of Thorlabs (Thorlabs, Newton, New Jersey, USA) 25mm steel rails and oriented towards nadir. The T440 uses a focal plane array uncooled microbolometer with a resolution of 320 x 240 pixels, a sensitivity range of 7.5 to 13μm, and a noise-equivalent temperature difference of 0.045 °C. The dimensions of the frame were 24” wide by 24” long by 18” tall. Four 325-watt Sunlite (Sunlite, Brooklyn, New York, USA) heat lamps with adjustable clamp mounts provide thermal stimulation. A stainless steel plate was used as the sample stage (stainless steel is highly reflective in infrared wavelengths,

minimizing heating due to the heat lamps and therefore maximizing contrast between the sample and background in collected videos). A USB-operated power relay module was used to activate and deactivate the lamps with high precision.

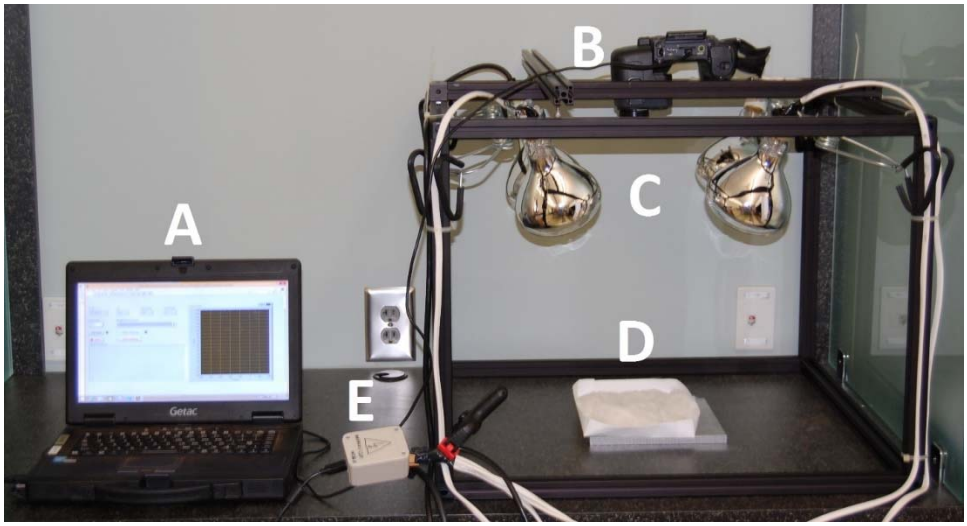

Figure 2.3. Pulsed thermography system physical components. A) Operating terminal; B) Thermal camera; C) Heat lamps; D) Sample stage; E) USB power relay for lamp control

A LabVIEW Virtual Instrument (VI) was created to automate the operation of this system. It consisted of three main tasks performed in parallel: activation and deactivation of the heat lamps, operation of the thermal camera, and memory management to rapidly acquire videos with no frame loss.

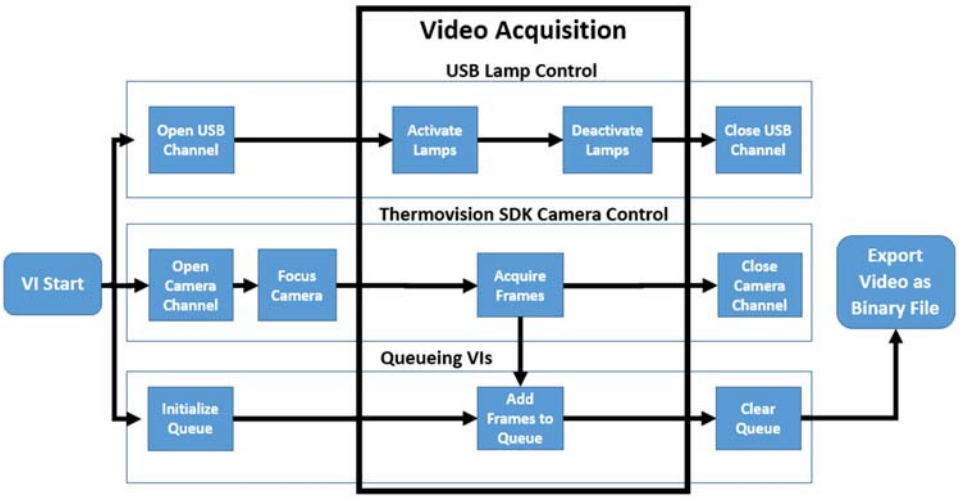

Figure 2.4. Pulsed thermography system automation virtual instrument flowchart

VIs from the FLIR ThermoVision SDK were used to operate the thermal camera and receive frames during video acquisition. To operate the USB power relay module, VIs were used which call functions from a third-party digital link library. VIs from LabVIEW's queueing system enabled high-speed data acquisition to memory. Lastly, videos were exported as binary files; other methods of export available in LabVIEW were not possible due to the relatively large file size of collected videos (approx. 300 megabytes).

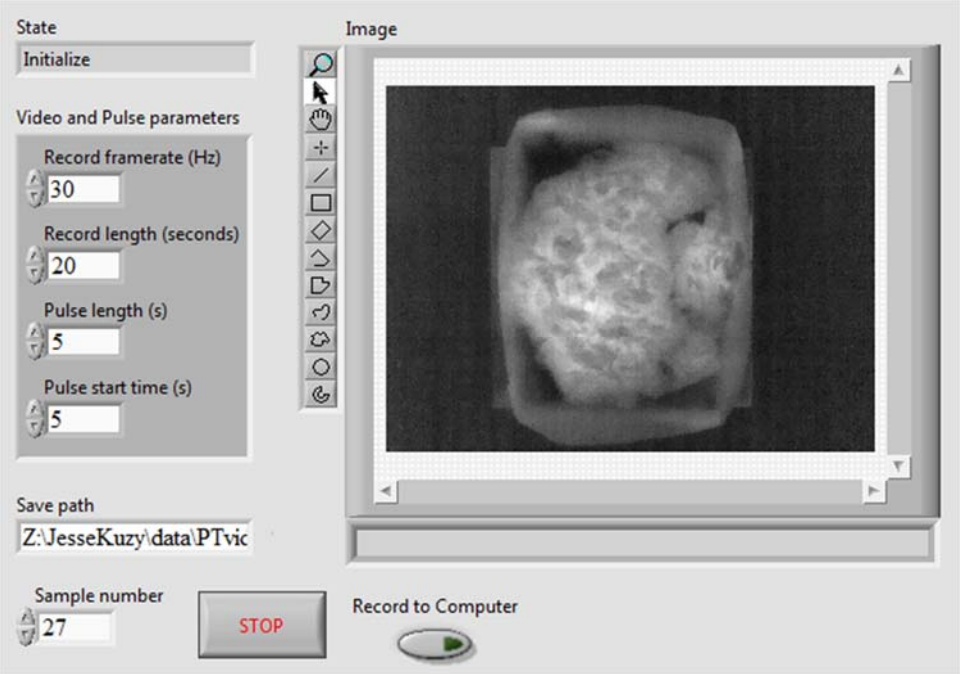

Figure 2.5. Pulsed thermography system automation virtual instrument front panel

Videos of pulsed thermographic analysis were collected in the following format: a front buffer of approximately 2.5 seconds; 5 seconds of thermal stimulation from the heat lamps; 10 seconds of cooling; and a rear buffer of approximately 2.5 seconds. Videos were collected during two sessions in 2016. A total of 240 videos, one each for each sample, were collected. The overall data processing pipeline was performed in four main steps (Figure 2.6): data collection, segmentation, feature extraction, and classification.

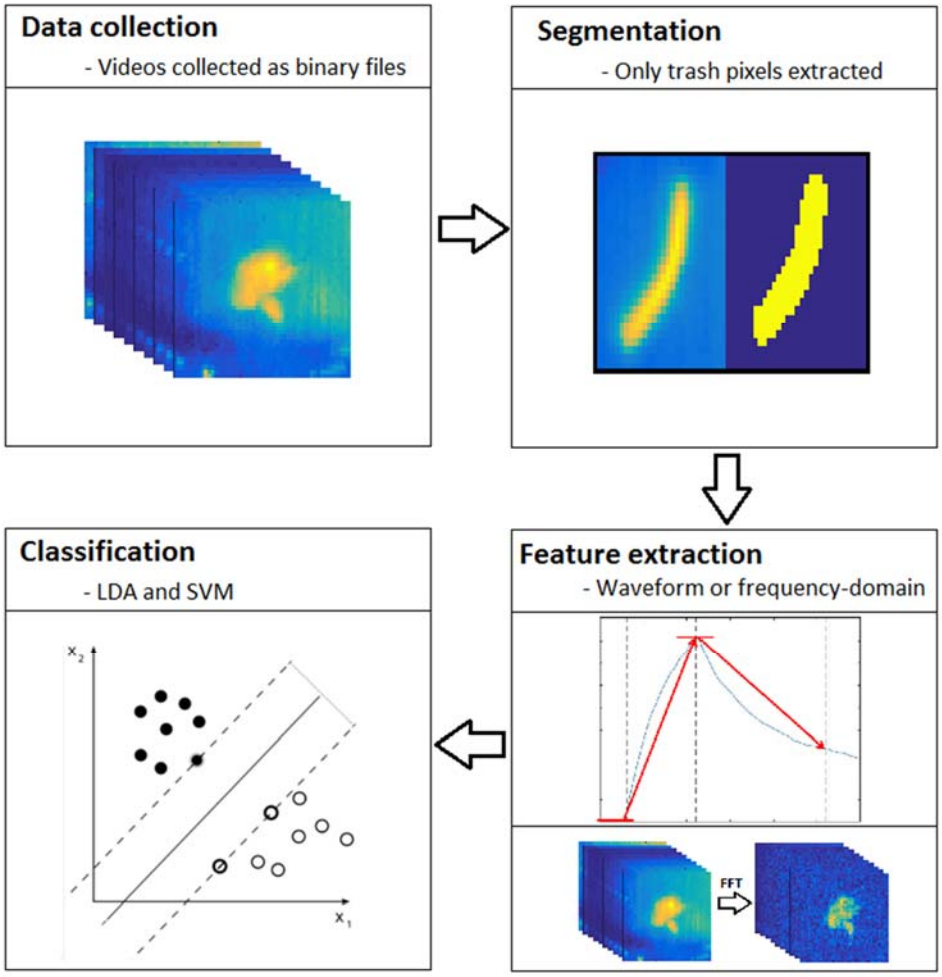

Figure 2.6. Diagram of data processing pipeline

2.2.3. Segmentation

Samples were segmented in the following fashion: For cotton samples, a 100-by-100-pixel window from the center of each video was extracted. For paper samples, a rectangular region from the center of each sample was selected, taking care to leave ample space between the selected region and the dark border marked with permanent marker on each sample. For all other samples, Otsu thresholding of the frame of peak temperature was used to create segmentation masks. Where necessary, the threshold was manually adjusted to produce accurate masks. All portions of the segmentation procedure were performed in MATLAB (The MathWorks, Inc., Natick, MA, USA).

2.2.4. Feature extraction

2.2.4.1. Frequency-domain features

Two sets of features were extracted from the segmented videos: pulse-phase thermography features of amplitude and phase values from complex components produced by Fourier analysis; and waveform features produced by analyzing the temperature waveforms of each pixel of each sample.

Fourier analysis of the samples was performed using MATLAB's fast Fourier transform (FFT) algorithm. This process decomposes the input signal into a sum of sinusoids expressed as complex phasors with evenly-spaced frequencies ranging from 0 to 30 Hz (the framerate of the acquiring device). Prior to Fourier analysis, each video was trimmed to only the rising and falling portions, with the pre- and post-stimulation buffers removed. This resulted in videos of precisely 450 frames. The input signal for Fourier analysis was the mean temperature of all of the sample's pixels during each frame, such as that shown in Figure 2.7. Following Fourier decomposition, a number of complex components equal to the number of frames in each video (450) were produced. According to the Nyquist theorem, all components with a frequency higher than ½ the collection frequency are aliased and therefore contain no additional information. Examination of the phase and amplitude values of the components confirmed this. Accordingly, the 225 components with frequencies higher than 15 Hz were discarded, leaving 225 components with frequencies from 0 Hz to 15 Hz. Each component, like all sinusoids, has an amplitude value and a phase value. Amplitude values were extracted by calculating the absolute value of each phasor, while phase values were determined by examining the angle of the phasor. The phase value of the 0-Hz component is always zero and was thus discarded. The final set of frequency-

domain features produced by this process was 224 phase values and 225 amplitude values for each sample.

2.2.4.2. Waveform features

In addition to the above frequency-domain features, which were produced by analyzing the entire waveform, consisting of the rising and falling portions together, waveforms were also analyzed in a split fashion. Since many prior applications [23,28] of pulse-phase thermography examine only the falling portion of the thermal signal, it is suspected that more meaningful frequency-domain features might be produced by independently performing Fourier analysis on the rising and falling portions of the full thermal signal. Additionally, this data may be of use for implementation in ginning facilities, where a possible point of examination is immediately after the cotton exits the dryers. This was conducted, producing 223 phase values (74 rising and 149 falling) and 225 amplitude values (75 rising and 150 falling). These will be referred to in analyses as "split features," as opposed to "whole features."

Four waveform features were manually extracted from each video: peak temperature, resting temperature, rising slope, and falling slope. When the thermal signal of each pixel of a foreign matter sample is averaged, the result is a temperature waveform such as that shown in Figure 2.7. This mean thermal signal was used to determine the frame of peak temperature, which is also the frame in which the lamps are deactivated, labeled as time 2; the mean temperature of all pixels during this frame was used as the peak temperature feature. The resting temperature was derived by averaging the mean temperature of the sample during the resting period of the video, region a. The rising slope was calculated by subtracting the peak temperature from the resting temperature and dividing by the length of the stimulation period b, 150 frames. The falling slope was derived

by subtracting the peak temperature from the mean temperature at time 3 and dividing by the length of region c, 300 frames.

Preliminary classification trials were performed in order to determine the optimal number of amplitude features to use. For each of the three sets of amplitude features (whole, rising, and falling), LDA and SVM classifiers were trained to perform both the detection (two-class, with one class being cotton and the other foreign matter) and identification (twelve-class, with cotton lint and each foreign matter type receiving a unique class label) tasks. Cumulative sets of features ranging from the lowest-frequency component's amplitude alone to a set consisting of the fifteen lowest-frequency amplitude values were used.

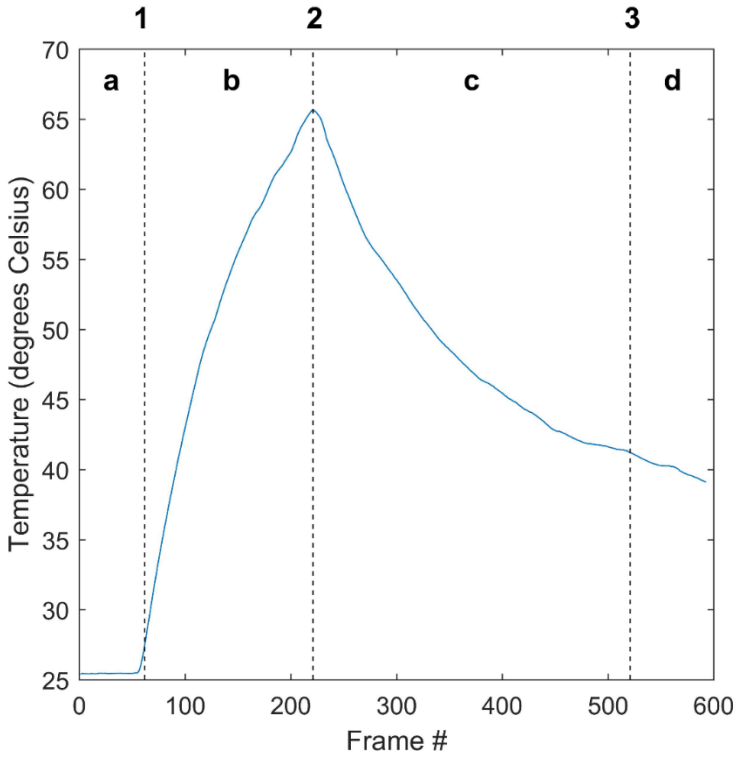

Figure 2.7. Segmented mean temperature waveform of cotton sample #4. a) resting stage / front buffer; b) thermal stimulation; c) cooling; d) rear buffer; 1) lamp activation; 2) lamp deactivation; 3) data cutoff

2.2.5. Statistical analyses and classification

In order to determine the degree of separation among the foreign matter types when all features in a given set are considered together, Hotelling's T-squared tests were performed for each pair of foreign matter classes. Additionally, canonical discriminant analysis was performed on each feature set. Both tests were performed using MATLAB's manova1 function.

Classification trials were performed in MATLAB using leave-one-out cross-validated support vector machine (SVM) and linear discriminant analysis (LDA) classifiers. Classification was performed using both waveform and amplitude features.

2.3. RESULTS

2.3.1. Waveform feature analysis

Examining the mean thermal waveform of each foreign matter type shows that there were clear differences in the mean thermal signals of the various foreign matter classes (Figure 2.2). For example, it is clear that the peak temperature of brown leaf samples, with a mean value of about 75 degrees Celsius, was substantially higher than that of seed coats, with a mean peak temperature of about 35 degrees Celsius. Examining other features of the waveform, it can be seen that bract and cotton samples, which achieved similar peak temperatures, had very different rates of cooling: the falling slope of the bract samples was substantially steeper than that of the cotton samples.

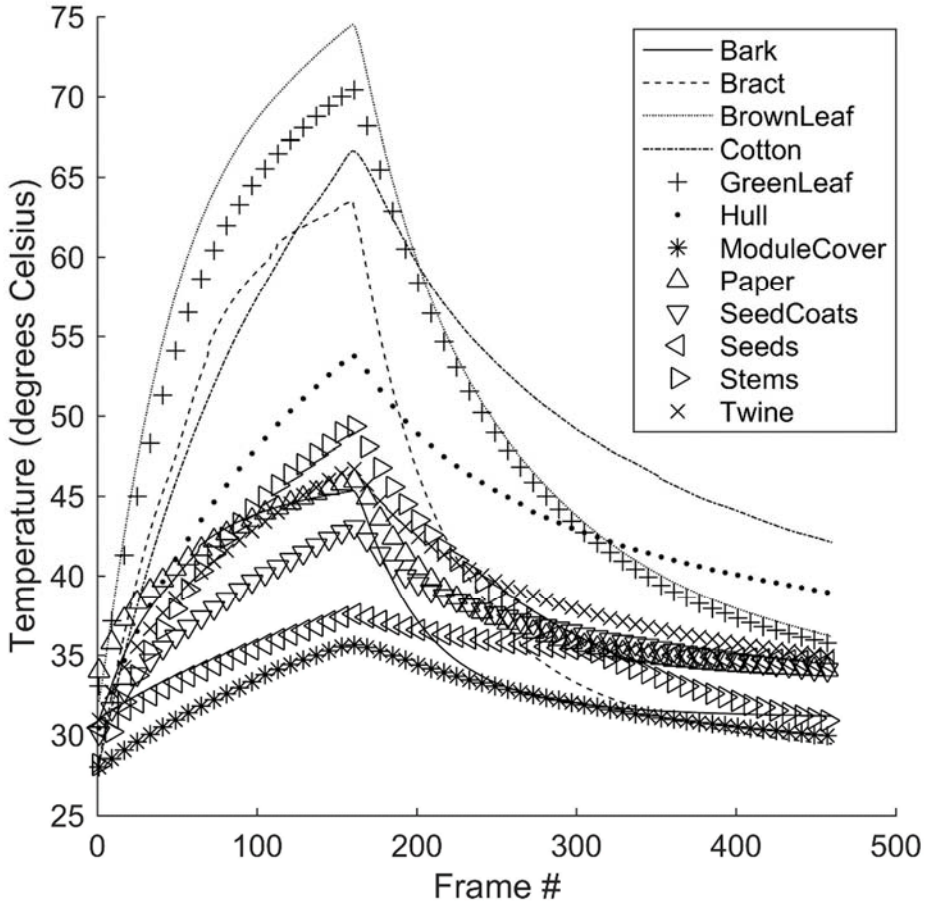

Figure 2.8. Mean thermal waveforms for all sample classes

The maximum temperature achieved by any sample class, approximately 75 degrees Celsius for brown leaf, is notable for being well below the threshold temperature at which it is considered unsafe to dry cotton, 150-175 degrees Celsius. Cotton may be dried at air temperatures of up to 120 degrees Celsius [29]. Since this well exceeds the maximum observed temperature of foreign matter in this study, it is reasonable to conclude that the magnitude of thermal change that results from drying will meet or exceed those observed in this study, and will therefore be sufficient to produce differences in thermal waveforms. This strengthens the possibility of implementing this technique without the need for exogenous heat sources. Conversely, this also suggests that the procedure, if conducted in isolation from the ginning process, poses no risk of overheating and damaging the cotton.

2.3.2. Frequency-domain feature analysis

Phase and amplitude data can be visualized by mapping the phase or amplitude values of a selected frequency component for each pixel in an image to a color map. The resulting images are known as phasegrams and ampligrams, respectively (Figure 2.9). In the thermal images it can be seen that bract, brown leaves, and green leaves achieve the highest temperatures, owing to the particulars of their geometry (broad and thin); ampligrams are primarily a reflection of this peak temperature, appearing as nearly identical to the thermal images, though with de-noised backgrounds. Phasegrams are more difficult to interpret: they represent the dynamics of how quickly differing regions heat and cool. So, for example, the edges of the module cover sample are clearly visible, implying a difference between the rate of heating and cooling between the edges and center. Likewise, samples with a linear geometry, such as bark, stem, and twine, all show a characteristic difference in phase values between the tips and the centers.

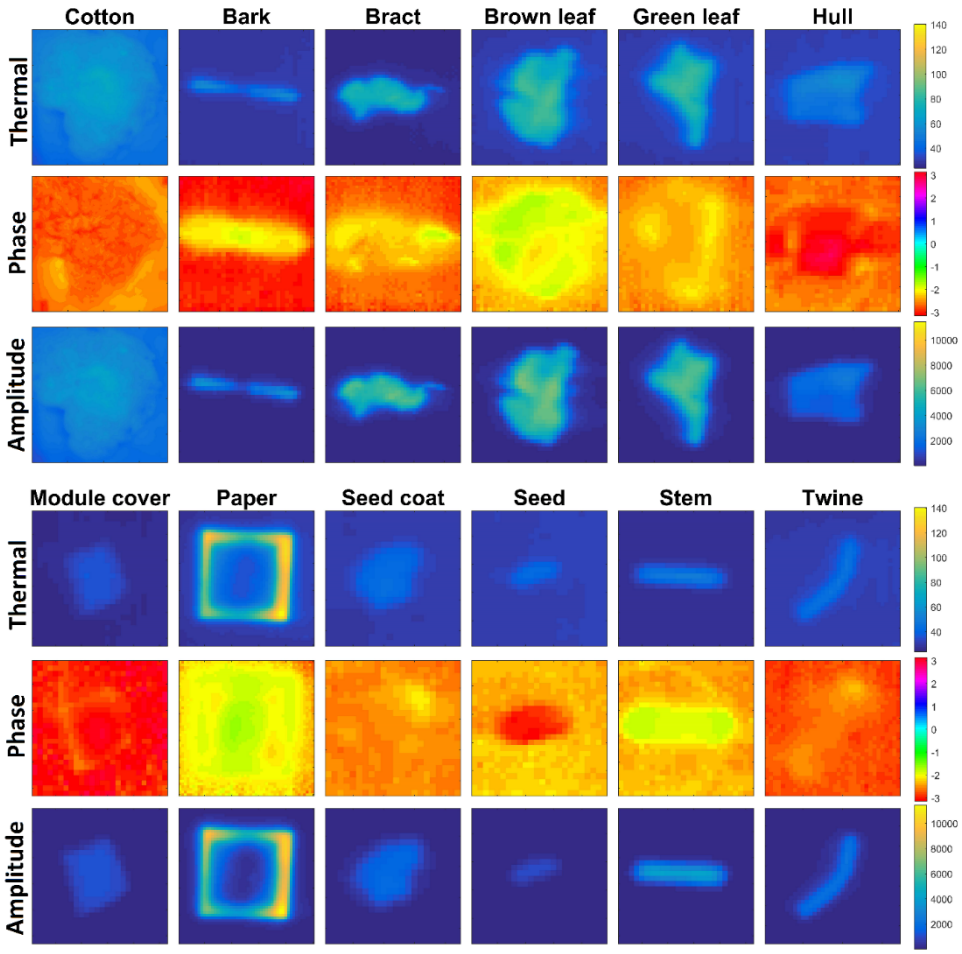

Figure 2.9. Thermal images, phasegrams, and ampligrams of each sample type

The accuracies produced by the preliminary computational tests were used to determine the optimal number of amplitude features in the range from 1 to 15 components (Figure 2.3). For the two-class task, accuracy was unstable until at least six components are used. For the twelve-class task, accuracy rose until nine components are used, then fluctuated. Based on these preliminary trials, the first ten amplitude features were selected to use in further classification trials and statistical analyses.

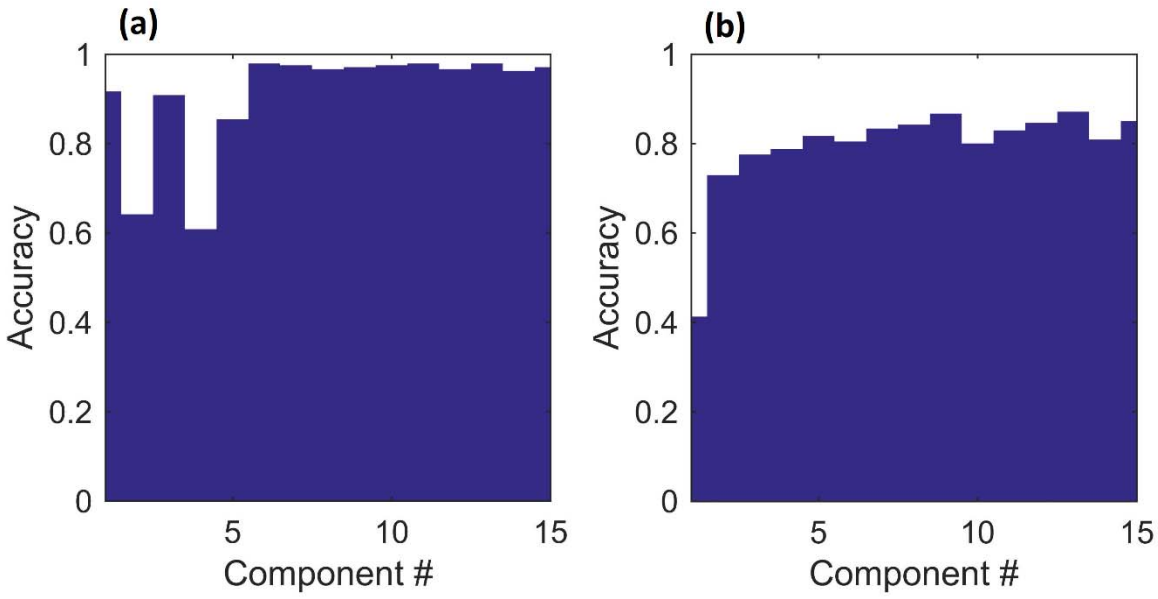

Figure 2.10. Results of preliminary amplitude feature classification trials using whole amplitude features and SVM classifiers. (a): Two-class task. (b): Twelve-class task

2.3.3. Statistical analyses

In the results of the paired Hotelling's tests (Figure 2.11), it can be seen that, for waveform features, almost every p-value between two groups was well below the stringent threshold $p = 0.001$. The sole exception was the test pairing leaves and brown leaves. However, even this pairing returned a p-value of 0.025, which is below the generally-accepted threshold of 0.05 for statistical significance. For amplitude features, all p-values were below 0.001, indicating statistically significant separation for all foreign matter types.

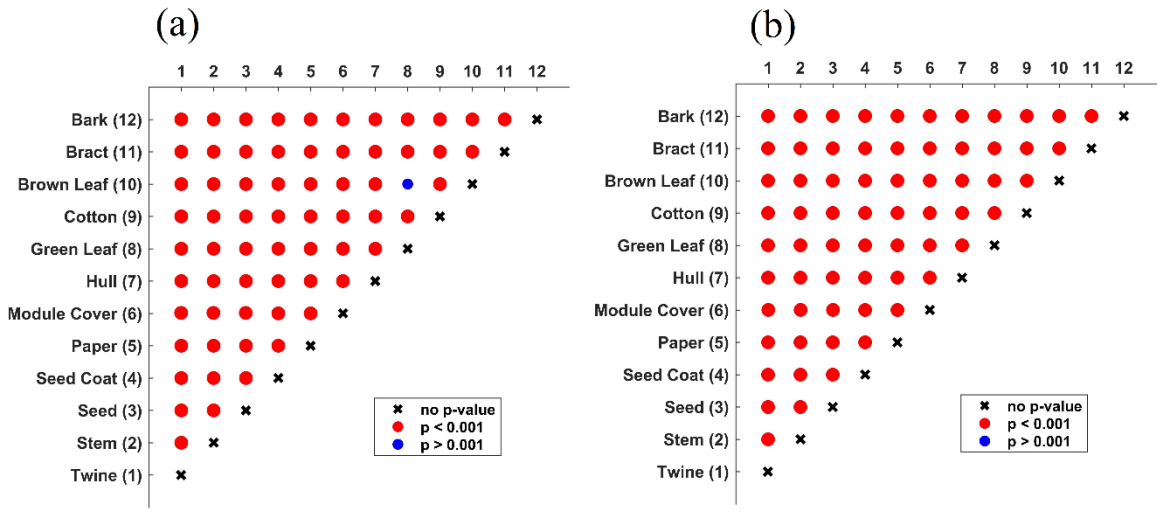

Figure 2.11. Pairwise p-values returned by Hotelling's T-squared test performed on waveform features. (a): waveform features; (b): amplitude features

2.3.4. Canonical discriminant analysis

The results of canonical discriminant analysis performed using the waveform features (Figure 2.12(a)) showed that there was good separation between many foreign matter types. Seeds, module cover, hull, and cotton samples were especially well-separated. Bract, brown leaves, and green leaves formed a combined cluster; given their biological and material similarity, this is unsurprising. Other foreign matter types were less well-separated: Paper, stems, and bark were mixed, and twine and seed coats were only moderately well-separated. It should be noted that when viewed in three dimensions, with the third canonical score considered, the separation of many of these clusters is improved.

The results of canonical discriminant analysis performed on waveform features showed similarly good separation between many classes (Figure 2.12(b)). What is most notable about this canonical scores plot is that it seems to be a horizontal reflection of the canonical scores plot of the waveform features. Again cotton, hull, module cover and seed samples were cleanly separated and clustered; bract, green leaves, and brown leaves formed a complex; seed coats were clustered

but not well-separated, and stems, bark, and paper were not well-separated. Although it is a subjective analysis, the strong similarity of the canonical score plots of the waveform and amplitude features seems to suggest that there is a large degree of overlap in the discriminating information contained by these feature sets.

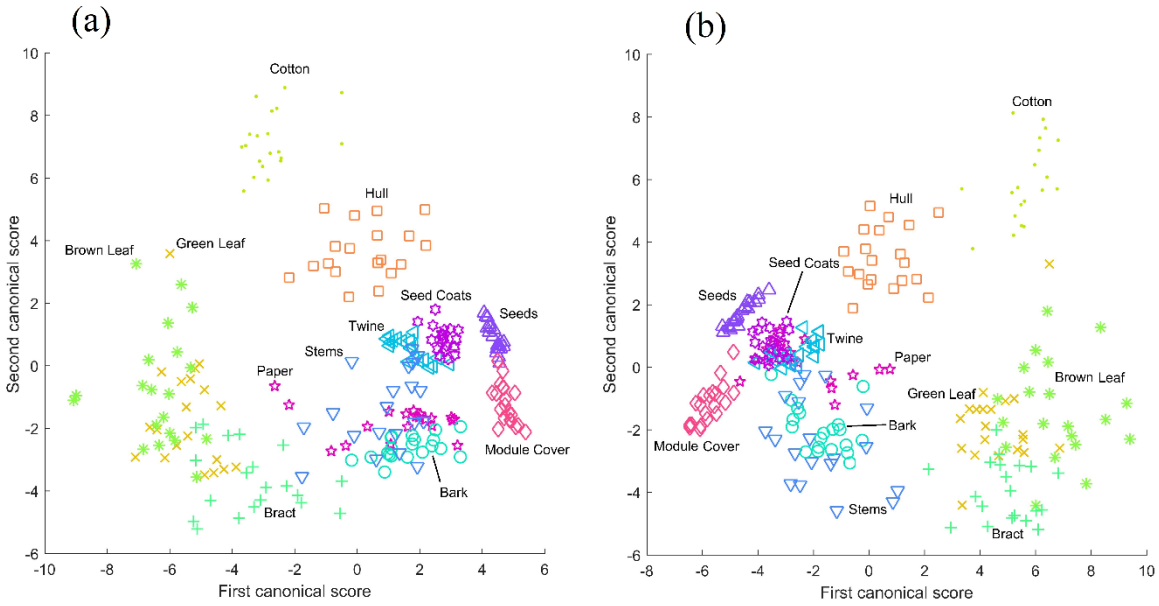

Figure 2.4. Canonical discriminant analysis scores plots from feature sets. (a): waveform features; (b): amplitude features

2.3.5. Classification results

The results of the classification trials produced very good results for the two-class detection problem, with more mixed results for the twelve-class identification problem (see Table 2.1). On the identification task, no combination of classifier and feature set produced an accuracy lower than 93%, while two trials returned accuracies above 99%. For the identification task, LDA achieved 90% accuracy of classification using either the waveform or whole amplitude features, while SVM provided 86.67% accuracy on whole amplitude features. For both detection and identification, the features which produced the best performance for SVM classifiers were whole amplitude features. With either classifier, whole amplitude features produced better accuracies

than either rising or falling amplitude features. In general, LDA and SVM accuracies on most tasks were comparable, with the most notable exception being the identification task when performed using waveform features.

The sharp decline in accuracy between the LDA and SVM performance on the identification task using waveform features may be a consequence of the inherent dimensionality of the classifiers. LDA, which linearly sums the constituent features to produce a final discriminating feature, is inherently one-dimensional; SVM, which projects features into additional dimensions, is multidimensional. It may therefore be the case that LDA is better-suited to feature sets with a lower dimensionality, such as the waveform feature set, while SVM is preferable for feature sets with increased dimensionality, such as the amplitude feature sets.

Table 2.1. Classification accuracies on two-class (detection) and twelve-class (identification) tasks using LDA and SVM classifiers and four feature sets

		Detection		**Identification**	
Feature set	**Number of features**	LDA	SVM	LDA	SVM
Waveform features	4	0.9958	0.9583	0.9000	0.7542
Whole amp 1:10	10	0.9917	0.9792	0.9000	0.8667
Rising amp 1:10	10	0.9500	0.9458	0.7292	0.7708
Falling amp 1:10	10	0.9625	0.9375	0.7500	0.7708

Examining the confusion matrix for the output of the identification task using LDA and waveform features (Figure 2.13 (a)), it can be seen that 5 foreign matter types were classified with 100% accuracy, and four with better than 90% accuracy. The two worst-performing classes, green leaves and brown leaves, had all errors as confusions of one another. Considering that there is no substantial difference between these classes in their impact on the quality of the cotton lint, this confusion may be excusable. Omitting these errors, which account for the majority of misclassified samples, produces an overall accuracy of 95.83%. The next-worst class, stems, had all three

misclassified samples erroneously labeled as bark. Considering that the surface of the stem samples used *was* bark, this is unsurprising. It is also notable that no cotton sample was misclassified, and no sample was misclassified as cotton: differentiation between cotton and all foreign matter samples was performed with perfect accuracy.

Classification errors were more mixed for the identification task using LDA and whole amplitude features (Figure 2.13(b)). Brown leaf was the most-misclassified class, for which the most common mislabeling was green leaves, but the inverse misclassification is not present. Bract samples were also misclassified often, with a wide variety of mislabelings. Just two classes were classified with perfect accuracy: cotton and seeds; but for this feature set, two samples were erroneously classified as cotton, which in an implemented system would amount to these foreign matter samples passing undetected. Although the overall accuracy was only marginally lower than that using waveform features, the misclassifications were more scattered and less easily explained, suggesting that amplitude features do not compare favorably to waveform features for the identification task.

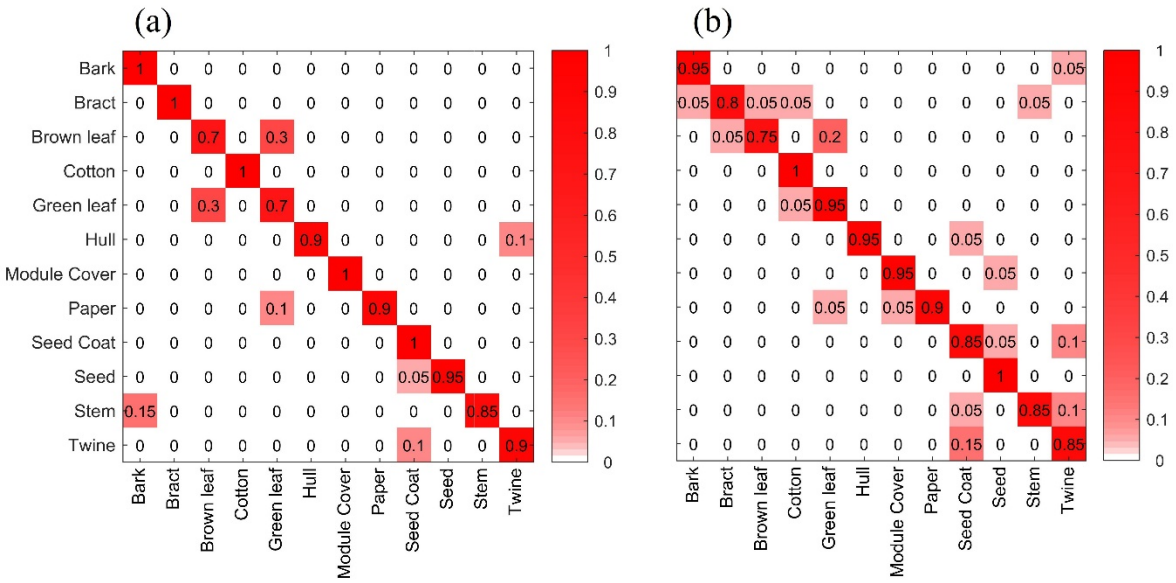

Figure 2.13. Confusion matrix for identification task performed using LDA with (a) waveform features and (b) amplitude features. Y axis is ground truth, X axis is classifier output.

These results compare well with the accuracies obtained by researchers using other methods: Fortier et. al.'s classification rates of 97% and 98% using FT-NIR spectrography are superior but are based on datasets with fewer foreign matter types (four and eight, respectively), and which did not include cotton. The maximal detection accuracy of 99.58% well exceeds Yang et al.'s detection accuracy of 92% [6,7], but does not top the 100% accuracy of Zhang et al. using shortwave infrared hyperspectral imaging [13]. Although the results for bark are superior to those of Zhang et al., those for stems are not, and it should be noted that Zhang et al. considered inner and outer bark and stem surfaces as separate categories, with most misclassification for these foreign matter types being the complementary category. Fortier et al.'s best results, those using the OPUS IDENT software with the NIR spectrum first derivative, surpass those for hulls and stems using either waveform or amplitude features, equal those for leaves using waveform features (Fortier et al. did not consider two colors of leaves but only one category). For seed coats their 91% accuracy

exceeds the 85% achieved with amplitude features but not the 100% produced by waveform features [9].

Since cotton is dried several times during ginning, it is possible that this thermal stimulation may produce data suitable for thermographic analysis. This would eliminate the need for additional exogenous heat sources. However, two reservations should be noted: First, cotton driers function on convective heating, not radiative heating, as was used in this study. This may entail changes to the thermal responses of the cotton and foreign matter, which warrants more in-depth studies. However, cooling should remain relatively unchanged, hence the examination in this study of amplitude features drawn only from the falling portion of the thermal waveform. Second, cotton drying temperatures are frequently adjusted according to the condition of the cotton being processed at the time. This variation necessitates a system which can adjust to multiple drying temperatures. These factors need to be considered in the implementation of such a system in a ginning facility.

2.4 CONCLUSION

The pulsed thermographic imaging system developed by this study was proven to be effective in discriminating between cotton foreign matter types. Classification tasks using LDA and SVM classifiers produce near-perfect detection of foreign matter using both waveform and frequency domain feature sets, and respectable accuracies of identification comparable to and in some cases exceeding those achieved by other groups. Waveform features provided perfect discrimination of cotton from foreign matter types using LDA classifiers. This technique is a natural fit for the cotton processing floor, on which cotton already undergoes significant rapid heating and cooling. These findings strongly recommend pulsed thermography as a method for the detection of foreign matter in cotton lint.

2.5 REFERENCES

1. Federation, I.T.M. Itmf cotton contamination survey. Zurich, Switzerland, 2014.
2. Himmelsbach, D.S.; Hellgeth, J.W.; McAlister, D.D. Development and use of an attenuated total reflectance/fourier transform infrared (atr/ft-ir) spectral database to identify foreign matter in cotton. *Journal of agricultural and food chemistry* **2006**, *54*, 7405-7412.
3. Ghorashi, H. Uster® hvi classic. Technologies, U., Ed. CI Singapore, 2004.
4. Frydrych, I.; Matusiak, M. Trends of afis application in research and industry. *Fibres and Textiles in Eastern Europe* **2002**, *10*, 35-39.
5. Xu, B.; Fang, C.; Huang, R.; Watson, M.D. Chromatic image analysis for cotton trash and color measurements. *Textile research journal* **1997**, *67*, 881-890.
6. Yang, W.; Li, D.; Wei, X.; Kang, Y.; Li, F. In *An automated visual inspection system for foreign fiber detection in lint*, 2009 WRI Global Congress on Intelligent Systems, 2009; IEEE: pp 364-368.
7. Yang, W.; Lu, S.; Wang, S.; Li, D. Fast recognition of foreign fibers in cotton lint using machine vision. *Mathematical and computer modelling* **2011**, *54*, 877-882.
8. Xu, B.; Fang, C.; Watson, M. Clustering analysis for cotton trash classification. *Textile research journal* **1999**, *69*, 656-662.
9. Fortier, C.A.; Rodgers, J.E.; Cintron, M.S.; Cui, X.; Foulk, J.A. Identification of cotton and cotton trash components by fourier transform near-infrared spectroscopy. *Textile Research Journal* **2011**, *81*, 230-238.
10. Fortier, C.; Rodgers, J.; Foulk, J.; Whitelock, D. Near-infrared classification of cotton lint, botanical and field trash. *Journal of cotton science* **2012**.

11. Jiang, Y.; Li, C. Detection and discrimination of cotton foreign matter using push-broom based hyperspectral imaging: System design and capability. *PloS one* **2015**, *10*, e0121969.

12. Guo, J.; Ying, Y.; Li, J.; Rao, X.; Kang, Y.; Shi, Z. Detection of foreign materials on surface of ginned cotton by hyper-spectral imaging. *Transactions of the Chinese society of agricultural engineering* **2012**, *28*, 126-134.

13. Zhang, R.; Li, C.; Zhang, M.; Rodgers, J. Shortwave infrared hyperspectral reflectance imaging for cotton foreign matter classification. *Computers and Electronics in Agriculture* **2016**, *127*, 260-270.

14. Gamble, G.R.; Foulk, J.A. Quantitative analysis of cotton (gossypium hirsutum) lint trash by fluorescence spectroscopy. *Journal of agricultural and food chemistry* **2007**, *55*, 4940-4943.

15. Mustafic, A.; Li, C. Classification of cotton foreign matter using color features extracted from fluorescent images. *Textile Research Journal* **2015**, *85*, 1209-1220.

16. Pai, A.S. X-ray microtomographic image analysis for identification of cotton contaminants. Texas Tech University, 2002.

17. Hellebrand, H.; Linke, M.; Beuche, H.; Herold, B.; Geyer, M. Horticultural products evaluated by thermography. *AgEng, Warwick* **2000**, 26-26.

18. Veraverbeke, E.A.; Verboven, P.; Lammertyn, J.; Cronje, P.; De Baerdemaeker, J.; Nicolaï, B.M. Thermographic surface quality evaluation of apple. *Journal of Food Engineering* **2006**, *77*, 162-168.

19. Van Linden, V.; Labavitch, J.; De Baerdemaeker, J. Bruising mechanism in tomato fruit: Concerted biomechanical and enzymatic action. *Communications in agricultural and applied biological sciences* **2003**, *68*, 11.

20. Manickavasagan, A.; Jayas, D.; White, N. Thermal imaging to detect infestation by cryptolestes ferrugineus inside wheat kernels. *Journal of Stored Products Research* **2008**, *44*, 186-192.

21. Danno, A.; Miyazato, M.; Ishiguro, E. Quality evaluation of agricultural products by infrared imaging method. *Memoirs Fac Agric* **1978**, *14*, 123-138.

22. Varith, J.; Hyde, G.; Baritelle, A.; Fellman, J.; Sattabongkot, T. Non-contact bruise detection in apples by thermal imaging. *Innovative Food Science & Emerging Technologies* **2003**, *4*, 211-218.

23. Baranowski, P.; Mazurek, W.; Witkowska-Walczak, B.; Sławiński, C. Detection of early apple bruises using pulsed-phase thermography. *Postharvest biology and technology* **2009**, *53*, 91-100.

24. Meinlschmidt, P.; Maergner, V. In *Detection of foreign substances in food using thermography*, AeroSense 2002, 2002; International Society for Optics and Photonics: pp 565-571.

25. Ginesu, G.; Giusto, D.D.; Märgner, V.; Meinlschmidt, P. Detection of foreign bodies in food by thermal image processing. *Industrial Electronics, IEEE Transactions on* **2004**, *51*, 480-490.

26. Gowen, A.; Tiwari, B.; Cullen, P.; McDonnell, K.; O'Donnell, C. Applications of thermal imaging in food quality and safety assessment. *Trends in food science & technology* **2010**, *21*, 190-200.

27. Maldague, X.; Marinetti, S. Pulse phase infrared thermography. *Journal of Applied Physics* **1996**, *79*, 2694-2698.

28. Ishikawa, M.; Hatta, H.; Habuka, Y.; Fukui, R.; Utsunomiya, S. Detecting deeper defects using pulse phase thermography. *Infrared Physics & Technology* **2013**, *57*, 42-49.

29. Mangialardi Jr, G.J.; Anthony, W.S. Retrospective view of cotton gin dryers. *Cordova, Tenn.: The Cotton Foundation, National Cotton Council* **2004**.

CHAPTER 3

BLUEBERRY BRUISE DETECTION BY PULSED THERMOGRAPHIC INSPECTION[1]

[1]J. Kuzy and C. Li. To be submitted to *Journal of Food Engineering.*

ABSTRACT

To maximize profitability of blueberry harvests, bruised berries must be detected and diverted from the fresh market product stream. The goal of this study was to develop a pulsed thermographic imaging system and explore its feasibility in non-destructively detecting bruised blueberries. In this paper, the design and construction of a pulsed thermographic imaging system was described. A total of 200 blueberry fruit samples from two southern highbush cultivars (Farthing and Meadowlark) were collected and bruising treatments were applied to half of the samples. Relevant features were extracted and were demonstrated to be significantly different between healthy and bruised fruit. Classification was performed using LDA, SVM, random forest, k-nearest-neighbors, and logistic regression classifiers. Accuracies of up to 88% and 79% were obtained for Farthing and Meadowlark berries, respectively. These results demonstrate the feasibility of pulsed thermography to discriminate between bruised and healthy blueberries.

3.1 INTRODUCTION

During harvesting and processing, blueberries are subjected to mechanical damage from a variety of sources: harvesting system actuators, drops into various containment bins, jolts during transit, the weight of other berries, and so on [1]. Mechanical damage may result in fruit internal bruising, thus reducing the quality and shelf life of the fruit. The profitability of blueberries is maximized when bruised and otherwise damaged fruits are successfully detected and diverted from the fresh market stream (in which consumers are attentive to the health of the fruits) to alternative product streams in which fruit quality is less important, such as baking mixes and preserves. Currently, the state-of-the-art method for blueberry internal bruising assessment is by bisecting the fruit and observing the discolored area in the cross-sections. This method is destructive and cannot be applied for quality inspection of all the fruit. Although soft-sorter systems typically installed in

a blueberry packing line can sort out soft fruit by letting berries land on a force sensor and measuring the firmness of the fruit, the system cannot directly measure fruit internal bruising [2]. The industry needs a non-destructive sensing technique to assess blueberry internal bruising and this paper explores the feasibility of pulsed thermographic imaging for this purpose.

Infrared thermography (IRT) is the measurement of infrared radiation emitted by an object. The fundamental mechanics of IRT are governed by the Stefan-Boltzman equation [3], Eq. 1:

$$P/A = \varepsilon\sigma T^4 \quad (1)$$

Where P is the power of emitted radiation in Watts, A is the area of the emitting surface in square meters, ε is the emissivity of the object, dimensionless, σ is the Stefan-Boltzman constant in W/m^2K^4, and T is the absolute temperature in °K. As temperature dominates the equation, a good estimate of the temperature of an object can be derived from the emitted radiation even when the object's emissivity is not known.

When the target of inspection is one which produces heat or has a stable heat distribution, thermography is used to monitor the production and distribution of heat throughout the target. Thermally inert objects at steady-state conditions achieve a homogenous temperature distribution, so only differences in emissivity are visible when passively observing the target. If the material property of interest cannot be correlated to changes in emissivity, active thermographic techniques may reveal more of the target's material properties [3]. In active thermography, the target is thermally stimulated and the thermal response of the target to the exogenous heat source is monitored. Analysis of the distribution of the exogenous heat throughout the target may then be performed to derive correlations to material properties.

One method of active thermography is lock-in thermography. In this method, the thermal

stimulation is sinusoidally modulated and applied for at least several periods of the cycle. Over time, the object should reach a steady state at which its temperature changes according to a sinusoid of the same frequency, but with some phase difference. Thermal video is recorded of the object during stimulation, and the phase angle between the stimulation and the object's response is calculated. This produces a phasegram which may reveal the object's thermal and material properties.

A similar technique is pulsed thermography. In this technique, a single square wave or Dirac pulse of thermal stimulation is applied to the target. The Fourier transform is used to decompose the time-series thermal response of the object into sinusoidal components. This produces sinusoidal components of varying frequencies, each with an associated amplitude and phase. Of the data present in the sinusoidal components, the amplitude and phase features can be used to delineate the properties of the object.

Prior research into fruit bruise detection by thermographic methods is limited. A foundational study demonstrating the visibility of bruises on apples, mandarin oranges, and Natsudaidai fruits in thermal images was conducted by Danno et. al. in 1997 [4]. It was found in that study that fruit bruises appeared to be between 0.2 and 1.0 degrees Celsuis cooler than surrounding tissues. Varith et. al. applied convective cooling and heating treatments to bruised apples, with bruises being visible in some samples [5]. However, this pattern was not always consistent in all samples tested. There were also considerable variations in accuracy of detection across cultivars. Varith's group was the first to articulate thermal window theory: the theory that bruised fruit tissues differ in their thermal diffusivity from healthy tissues, specifically, that bruised tissues have a higher thermal diffusivity. Bruising ruptures cell walls and releases fluid from cells' interiors into the extracellular matrix, creating a pathway for thermal conduction through bruised tissues. When a thermal

stimulus is applied to a bruised berry, heat diffuses more quickly from the surface towards the cool interior, resulting in a smaller magnitude of temperature increase at the surface compared to a healthy berry. This provides the theoretical basis for discrimination between bruised and healthy fruit tissues in active thermographic inspection techniques. Baranowski et. al. [6] applied active thermographic inspection techniques to bruised apples by heating them with halogen lamps, and produced clear visualizations of bruises in thermal, amplitude, and phase images, as well as demonstrating phase differences between bruises of differing depths. A follow-up study in 2012 [7] applied both lock-in and pulsed thermographic techniques to bruised apples, once again producing visualizations of bruises and providing information about bruise depth. Most recently, Kim et. al. [8] applied lock-in techniques to bruised pears, with bruises being clearly visible in phase images. Measured variances in phase values with varying bruise depths were observed, and aligned precisely with variances predicted by a photothermal model.

To the best of the authors' knowledge, no studies have ever been published on thermographic detection of bruises in blueberries, or berries of any kind. Given the demonstrated ability of thermographic inspection to detect bruises in other fruits (mostly fruits larger than berries), it is worthwhile to explore whether the technique applies to small fruits such as blueberries. Additionally, thermographic inspection may be well-suited to blueberry inspection in particular due to significant temperature changes which occur to the berries during processing. Freshly-harvested berries moved from a hot field (30-40 ^{o}C) to a climate-controlled packing facility and cold storage (1-5 ^{o}C) will experience up to 40 ^{o}C of temperature change. It is possible that a thermographic inspection system appropriately located downstream from a thermal stimulus to the berries could exploit pre-existing temperature changes in berry processing, obviating the need for a system which provides its own thermal stimulus.

The overall goal of this study was to demonstrate that pulsed thermographic imaging analysis can be used to discriminate between healthy and bruised blueberries. The specific objectives were to: 1) develop a custom pulsed thermographic imaging acquisition system to collect pulsed thermographic images of bruised and healthy berries; 2) extract effective features in both the time domain and the frequency domain to delineate differences between bruised and healthy berries; and 3) discriminate between bruised and healthy berries on the basis of these features using machine learning techniques.

3.2 MATERIALS AND METHODS

3.2.1 Pulsed thermographic imaging system

A pulsed thermographic imaging system was created to facilitate data collection (Figure 3.1). The physical components of the system consisted of: a FLIR T440 thermal camera (FLIR Systems, Wilsonville, Oregon, USA); four 325-watt Sunlite heat lamps (Sunlite, Brooklyn, New York, USA); a Teflon sample stage; a USB-operated power relay; an operating terminal (Dll Inc., Round Rock, Texas, USA); and a frame constructed of 25mm optical ThorLabs optical railing, not shown (Thorlabs, Newton, New Jersey, USA).

Selection of an appropriate sample stage is an important consideration: The stage should provide a smooth background to facilitate segmentation. It should be reflective in the infrared range to minimize absorbed radiation, and therefore accumulation of heat over time, but this reflectiveness should be diffuse, rather than specular, to avoid visible reflections of the thermal camera and heat lamps. Lastly, the stage should have significant thermal inertia, either due to sheer mass or high heat capacity, in order to avoid drastic temperature fluctuations during data collection. After preliminary tests, the Teflon sample stage was selected because it never exceeded an observed temperature of approximately 307 K.

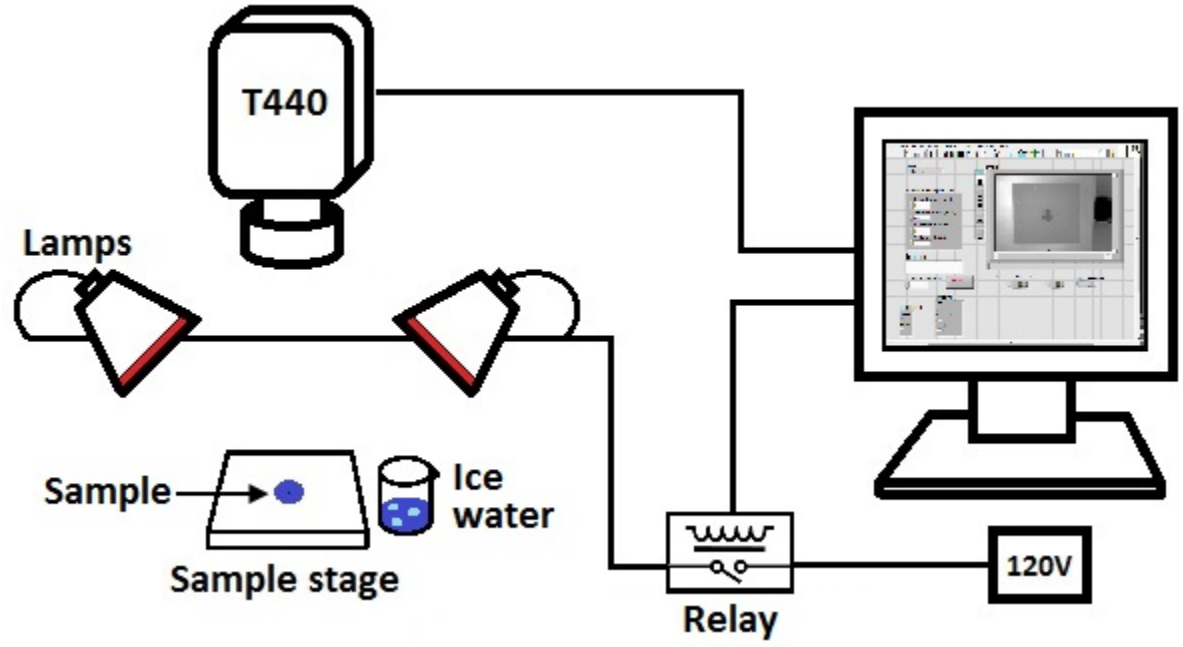

Figure 3.1. Diagram of the pulsed thermographic imaging system

The imaging system was controlled by a LabVIEW (National Instruments, Austin, Texas, USA) Virtual Instrument (VI) created for previous studies [9]. The main functions of the VI were: 1) Operation of the thermal camera by a source development kit provided by FLIR; 2) Precise activation and deactivation of the heat lamps by a USB-controlled power relay using a third-party digital link library; 3) Management of the high data volume using memory queueing sub-VIs to prevent frame loss; and 4) Export of the collected data as binary files. Figure 3.2 shows the front panel of the VI.

Several additional features were incorporated into the pulsed thermographic system control VI for this study. Importantly, an unintended and detrimental feature of previous VIs was compensated for: while a connection between an operating terminal and the T440 is maintained, the T440 ceases automatic initiation of its internal recalibration procedure. Like all uncooled thermal cameras, the temperature of the thermal camera and its detector can fluctuate due to

ambient conditions and prolonged operation. This causes the sensitivity of the camera to fluctuate, changing its readings. In order to compensate for this, the T440 periodically closes an internal shutter, references its internal thermometer, and adjusts an internal parameter to rectify the readings. When this procedure is disabled, the readings taken by the camera drift during continuous operation, at times severely. Commands were incorporated into the VI to instruct the thermal camera to perform internal shutter calibration following each sample collection; however, the camera performs recalibration only when it both receives a recalibration command and detects a significant change in its internal temperature. Consequently, the T440 did not perform internal recalibration following every sample collection, as desired, but only periodically, a total of approximately twenty times during data collection. In addition, an auditory cue was added following completion of one video collection, to assist the operator in timely exchange of samples and maintaining a high throughput rate.

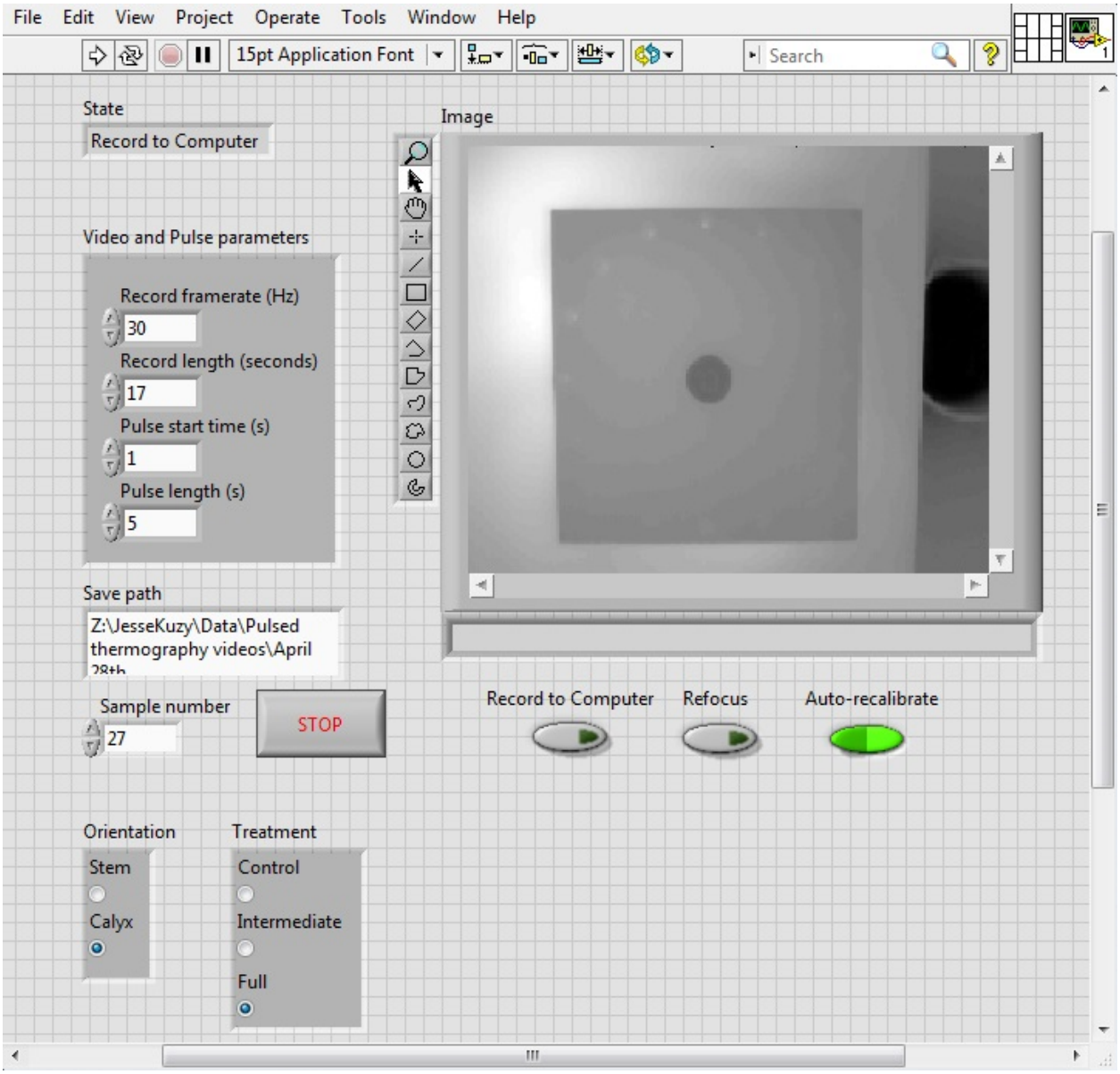

Figure 3.2. Front panel of pulsed thermographic system operation VI

3.2.2 Sample preparation

Two cultivars (Farthing and Meadowlark) with 250 berries each were hand-picked from Straughn Farms in Waldo, FL on April 27th, 2017. Samples were immediately stored in a cooler with ice and transported back to the Bio-Sensing and Instrumentation Laboratory at the University of Georgia. Berries were sorted and unripe, shriveled, damaged, or otherwise defective berries

were discarded. 100 Meadowlark and 100 Farthing samples of good quality and non-extremal size were selected for use in the study. Samples were treated the same evening, that of the 27th, approximately 6 hours after picking. Two treatment groups of 100 berries each were created: a control group and a bruised group, each containing 50 Farthing and 50 Meadowlark berries. Bruised group berries were poured between two plastic containers from a height of four feet a total of eight times. Control group berries were not treated. Samples were organized on wooden sample holders, covered with aluminum foil (avoiding heating from the ambient light), and set in an air-conditioned room for 15 hours for bruises to mature.

3.2.3 Thermal image acquisition

Prior to imaging, the thermal camera was warmed up for 30 minutes, avoiding potential fluctuations in temperature of the detector due to continuous operation. Videos were collected in a strict format with a total length of 17 seconds. At one second after initiating recording, the heat lamps were activated. At six seconds, they were deactivated, for a total pulse length of five seconds. Ten seconds of cooling curve were then collected, and lastly an additional second of buffer, to guard against inadvertent truncation. As an additional protection against sensor drift or miscalibration, a glass of well-mixed ice water was placed in the field of view of the camera for each trial. Subsequent examination of the apparent temperatures of the ice water confirmed that there was no significant variation in the sensitivity of the thermal camera throughout data collection.

Preliminary experiments showed that the imaging area becomes hotter as imaging proceeds, raising a concern that if one treatment group is imaged after another, it will be exposed to hotter ambient conditions, particularly from the hot sample stage and lamps, potentially introducing a confound into the data. For this reason, samples were collected in an interlaced fashion: Control

group sample 1 was imaged first, followed by bruised group sample 1, then control group sample 2, and so on. Calyx sides were imaged first, followed by stem sides, for two videos per berry, producing 400 videos in total.

3.2.4 Destructive evaluation and bruise area index derivation

Following collection of thermal data, all samples were destructively evaluated by slicing them in half down a calyx-stem axis and collecting color images of the interior (Figure 3.3). This was done in order to ensure that treatments were appropriately administered. In order to validate results against ground truth data, destructive evaluation images of berries were analyzed to produce a bruise area index feature. This feature is the percentage of pixels of a berry's destructive evaluation image judged to correspond to bruised tissues. The Sobel edge detection method was applied to destructive evaluation images to produce an edge detection image; circles were then fit to this image to produce preliminary masks because the shape of berry samples could be approximately described as two overlapping offset circles. Masks were cleaned up and segmented from one another manually using a custom segmentation wizard in MATLAB (The MathWorks, Inc., Natick, MA, USA). After observing that the contrast between bruised and healthy tissues was most distinct on the green channel, the green channel pixel intensities of the segmented destructive evaluation images was examined, and a threshold intensity value of 113 (on a range of 0-255) was selected. The number of pixels having an intensity of less than 113 on the green channel was taken as the number of bruised pixels for each berry. The dividend of the number of bruised pixels and the total number of pixels in the berry image was taken as the bruise area index.

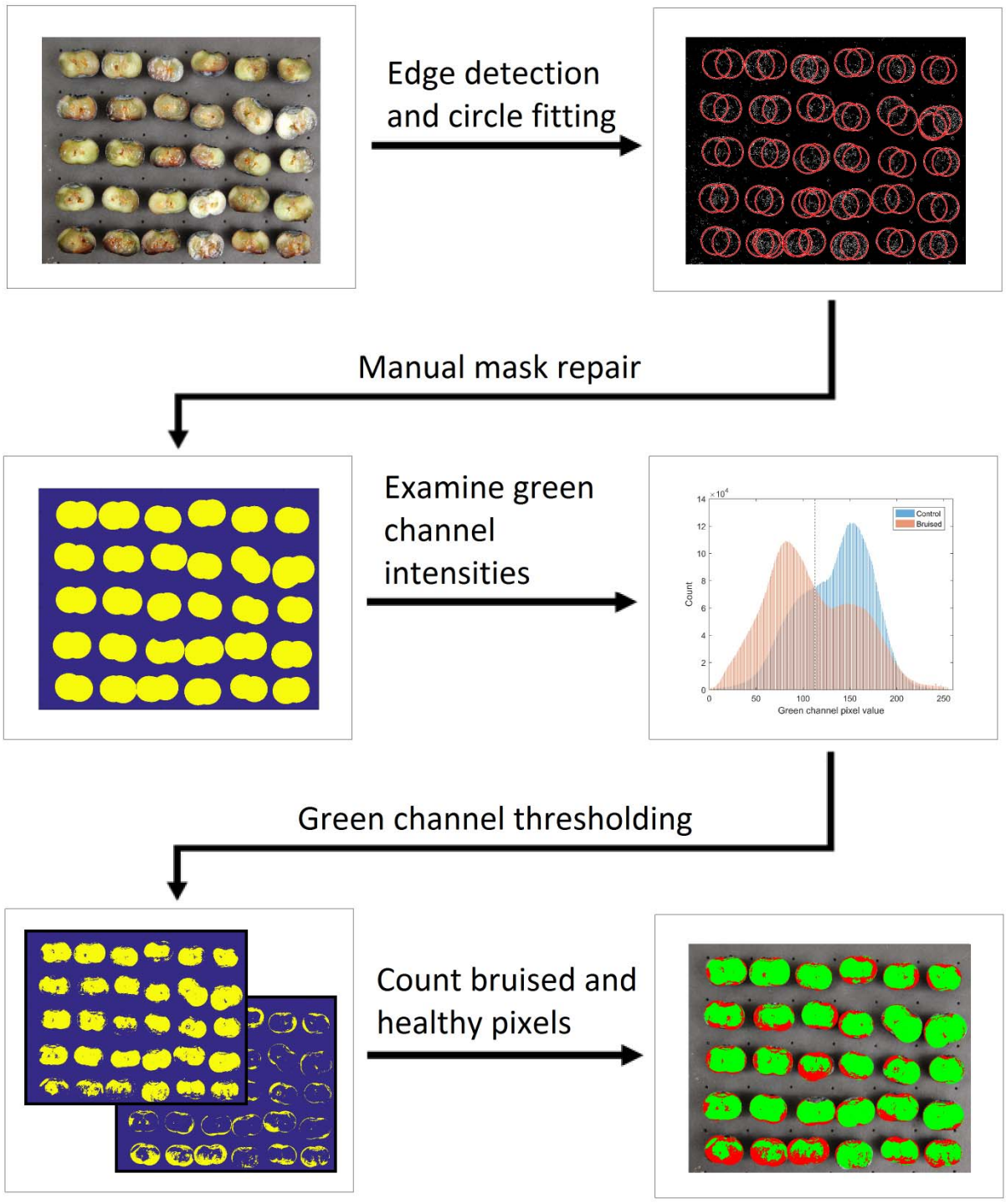

Figure 3.3. Illustration of bruise area index derivation

3.2.5 Thermal image processing

3.2.5.1 Preprocessing

Berries which did not appear in the destructive evaluation images to have received proper treatment, such as control group berries with bruises or bruised group berries with little damage, were removed from the dataset. A total of 11 bruised group berries were removed, leaving 189 berries in the dataset, for a total of 378 thermal videos. The 378 videos were further processed with masking, feature extraction, statistical analyses, feature selection, and classification (Figure 3.4).

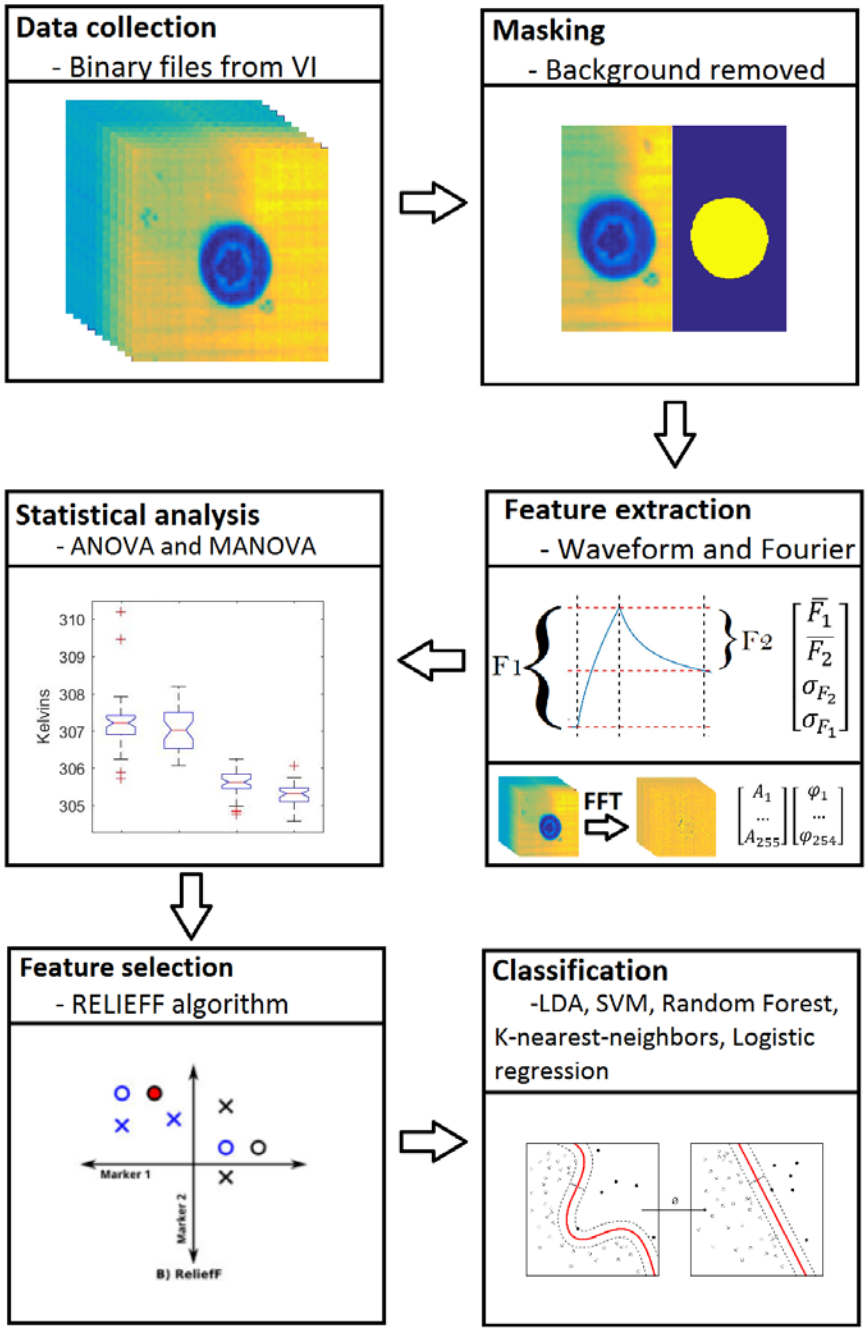

Figure 3.4. Data processing pipeline for the acquired thermal videos

3.2.5.2 Feature extraction

In each thermal video, the berry sample mask was generated by thresholding the peak temperature frame (Frame #186), and was then applied to each frame in the video to extract only

berry pixels. All extracted berry pixels were averaged together spatially, producing a temperature time series (Figure 3.5). From these mean temperature time series, two classes of features were extracted: time-domain waveform features and frequency-domain features.

Six waveform features were extracted from each temperature time series, including the starting and peak temperatures and the mean and standard deviation of rising and falling waveform features. The starting temperature was the mean temperature of all frames prior to time 'a', and the peak temperature was the mean temperature at time 'c' (Figure 3.5). The rising waveform feature was the difference between the peak temperature and starting temperature, or the total mean temperature increase during the heating phase. The falling waveform feature was the difference between the peak temperature and cooled temperature (the temperature at time e in Figure 3.5), or the total mean temperature decrease during the cooling phase. Since each pixel in each video has its own waveform, each pixel therefore also has its own waveform features. Both the mean value of the rising and falling waveform features across the visible pixels of a sample and the standard deviation of the features were extracted.

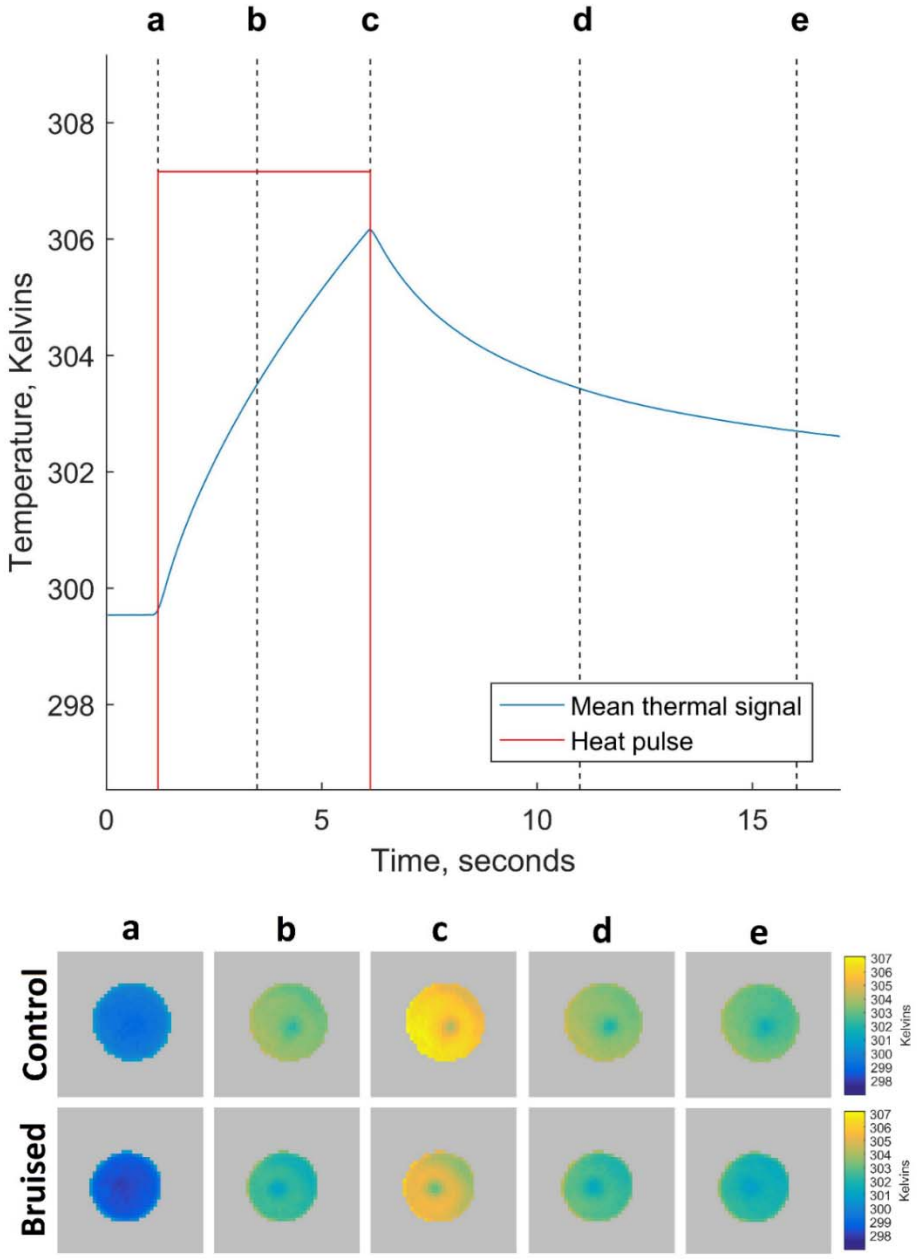

Figure 3.5. Mean thermal waveform of all samples with extracted thermal images for representative bruised and healthy samples. (a) Lamp activation; (b) Heating midpoint; (c) Peak temperature/lamp deactivation; (d) Cooling midpoint; (e) Cooling endpoint/data termination

To extract frequency-domain features, the thermal time series were first processed by Fast Fourier Transform (FFT) using the algorithm native to MATLAB. This produces a number of components in the complex domain equal to the number of frames in each video, that is, 511. The frequencies of these sinusoidal components are evenly-spaced from zero to the framerate of the thermal camera, 30 Hz. According to the Nyquist theorem, half of these components are aliased, and therefore contain no information that is not present in the other half. As such, 255 components were discarded, leaving the lowest-frequency 256 components. From each of these components, the phase and amplitude values were extracted by taking the angle and magnitude, respectively, of the complex phasor. Since the phase of the zero-frequency component is always equal to zero, this was also discarded, leaving 256 amplitude values and 255 phase values for each sample. Due to the relatively long timescale of the experiment, low-frequency phenomena were emphasized; consequently, only the first ten values from the ten lowest-frequency components were used in the following processes.

3.2.5.3 Statistical analyses

This study aimed to explore the feasibility of using pulsed thermographic imaging to identify bruised blueberries, so it was important to minimize (or eliminate) effects due to experimental factors other than the bruising treatment. As preliminary experiments showed the mean rising waveform was a good indicator of differentiating berry samples, an analysis of variance (ANOVA) test was performed on this feature to test the effects of all potential experimental factors (bruise treatment, sample orientation, and cultivar). The result recommended the examination of data subsets divided by orientation and cultivar (Table 3.3 in Supplementary Materials), and thus the following statistical analyses, feature selection, and classification trials were executed for individual data subsets.

ANOVA tests were firstly conducted to evaluate the usefulness of individual waveform features in identifying bruised blueberries. To further prove the efficacy, Pearson correlation analyses were also performed between the waveform features and bruise area index derived from destructive evaluation. In addition to the univariate features, the bruise identification power was examined using multivariate analysis of variance (MANOVA) for feature sets. Three sets of features were examined: waveform, amplitude, and phase. The waveform feature set consisted of the rising and falling waveform features plus their respective standard deviation features. The amplitude and phase feature sets consisted of the ten lowest-frequency values available for each feature set, plus the ten corresponding standard deviation features (that is, the standard deviations of the amplitude and phase values for each component when considered across all the pixels of each sample). ANOVA and MANOVA tests were performed in SAS (SAS Institute Inc. Cary, NC, USA), whereas Pearson correlation analysis was performed in MATLAB.

3.2.5.4 Feature selection

Feature selection was performed using the RELIEFF algorithm implemented in WEKA (The University of Waikato, Hamilton, New Zealand). The RELIEF algorithm iteratively updates a vector of feature merit scores based on the Euclidian distance between same-class and different-class samples in the feature space. Features which contribute to the clustering of same-class samples are updated with increased merit scores, while features that contribute to the clustering of different-class samples are penalized. Feature rankings are returned by ordering features according to their merit scores. RELIEFF is an updated version of this algorithm which uses Manhattan rather than Euclidian differences as the basis of its score adjustment, iterates exhaustively through all samples, and checks against more same-class and different-class samples. For these analyses, the following parameter values were used: number of neighbors checked, k, was 10; the neighbor

influence parameter σ was 2; weighting by distance was set to false; and all samples were used for attribute estimation. Based on the results, additional optimal feature sets were assembled and used for classification.

3.2.5.5 Classification

Feature sets were classified using five classifier systems: linear discriminant analysis (LDA), support vector machine (SVM), random forest, logistic regression, and K-nearest-neighbors (KNN). For SVM classifiers, four variants were tried: Two trials were performed with normalized data, and two with unnormalized data; and within each set of two, one classifier employed a linear kernel, and the other a radial basis function (RBF). Classification trials were performed using ten-fold cross-validation, with the three full feature sets (waveform, amplitude, and phase) and additional optimized feature sets from feature selection. The mean accuracy with its standard deviation was obtained for each trial to compare performance among classifiers. In addition, Cohen's Kappa statistics were calculated for performance evaluation to compensate for the unbalanced Meadowlark dataset (shown in Supplementary Figure 3.5). All trials and performance comparisons were performed in WEKA.

3.3 RESULTS AND DISCUSSION

3.3.1 Basic feature analysis

Examining the raw thermal waveforms (Figure 3.6), it can be seen that the treatment groups begin at roughly the same starting temperature, but peak and cooled temperatures are higher for control group berries. However, large variations were also observed within each treatment group, making a quick visual discrimination not an easy task. Among phase values, the mean value for most components is in the range of 1.2-2.2 radians, while those for the second component were

centered on a mean near -3 radians; phase values for the second frequency component have therefore been omitted from the figure, in order to increase the visibility of differences in other components; for example, it can be seen that component 9 has a larger difference between mean treatment group phase values than other components. In the case of amplitude values, the magnitude of the values decreases logarithmically with increasing component frequency, necessitating the omission of the three lowest-frequency components in order to produce a scale on which differences between the means are intelligible. It can be seen that the values for component six, and to a lesser degree, component five, show larger mean differences than other components. Similarly to thermal signals, the differences between frequency-domain features are accompanied by relatively large standard deviations that motivate more detailed inspection and analysis.

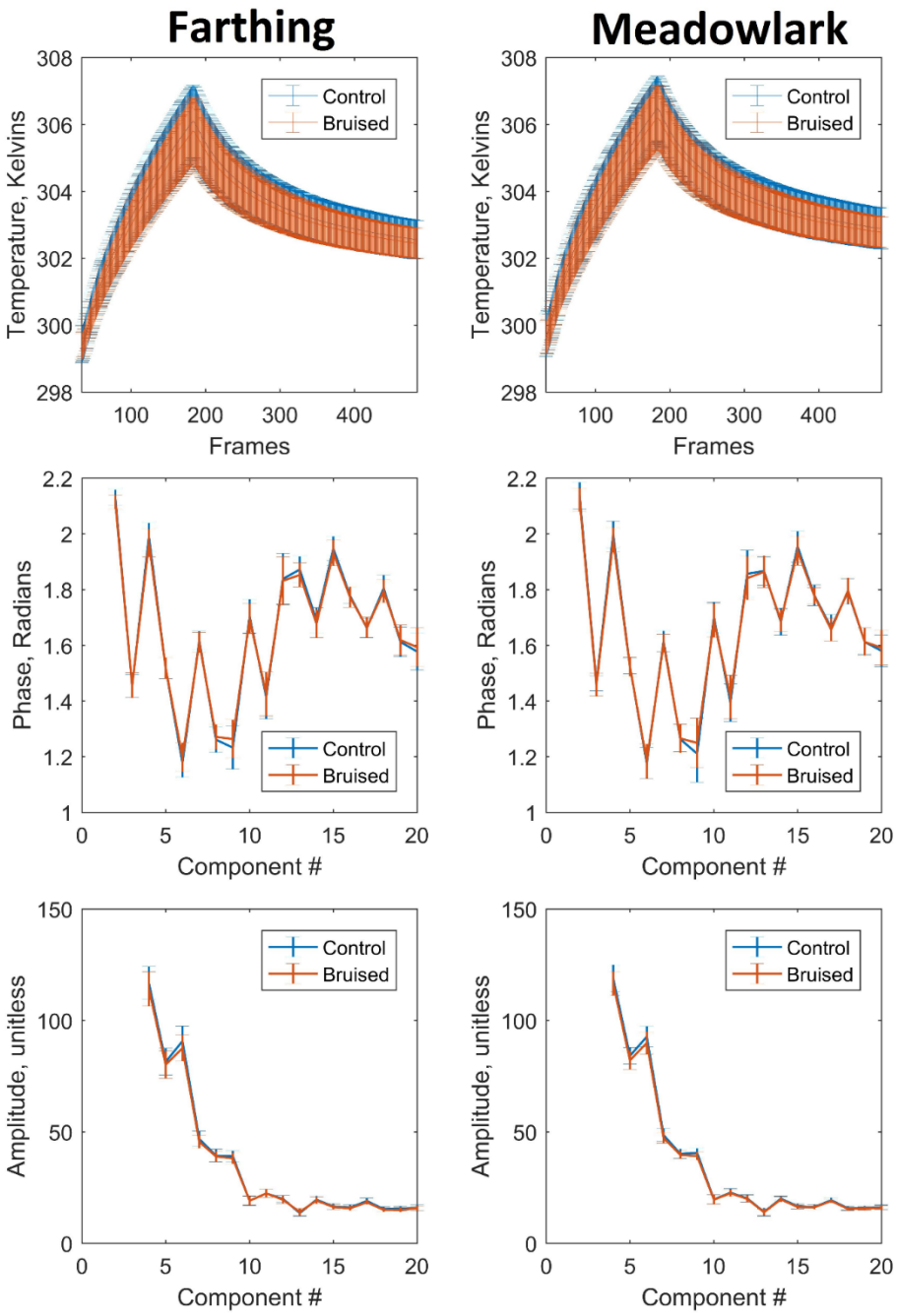

Figure 3.6. Mean thermal waveforms, mean phase values, and mean amplitude values for bruised and healthy treatment groups, separated by cultivar.

3.3.2 Thermal image visualizations

For the purposes of feature extraction, the Fourier transform was performed on the mean time

series for each sample, but it can also be performed on the individual pixel time series in each video. The phase and amplitude values for a given frequency component can then be mapped to color values and displayed, producing images known as phasegrams and ampligrams, respectively. In some applications, defects such as cracks or voids in rigid parts, or bruises in fruits, can be observed in these images. In this case, color images reveal no obvious differences between the bruised and healthy berry, but thermal images taken from the time of peak temperature show a clear temperature difference, with the control berry being hotter (Figure 3.7). Ampligrams, tending to resemble de-noised thermal images, likewise show a higher magnitude of amplitude values for the healthy berry. Phasegrams primarily highlight the different tissues of the samples, with the pedicle being distinct, and calyxes shown clearly in calyx-end images. Significant differences between the mean phase values of bruised and healthy berries are not visually apparent.

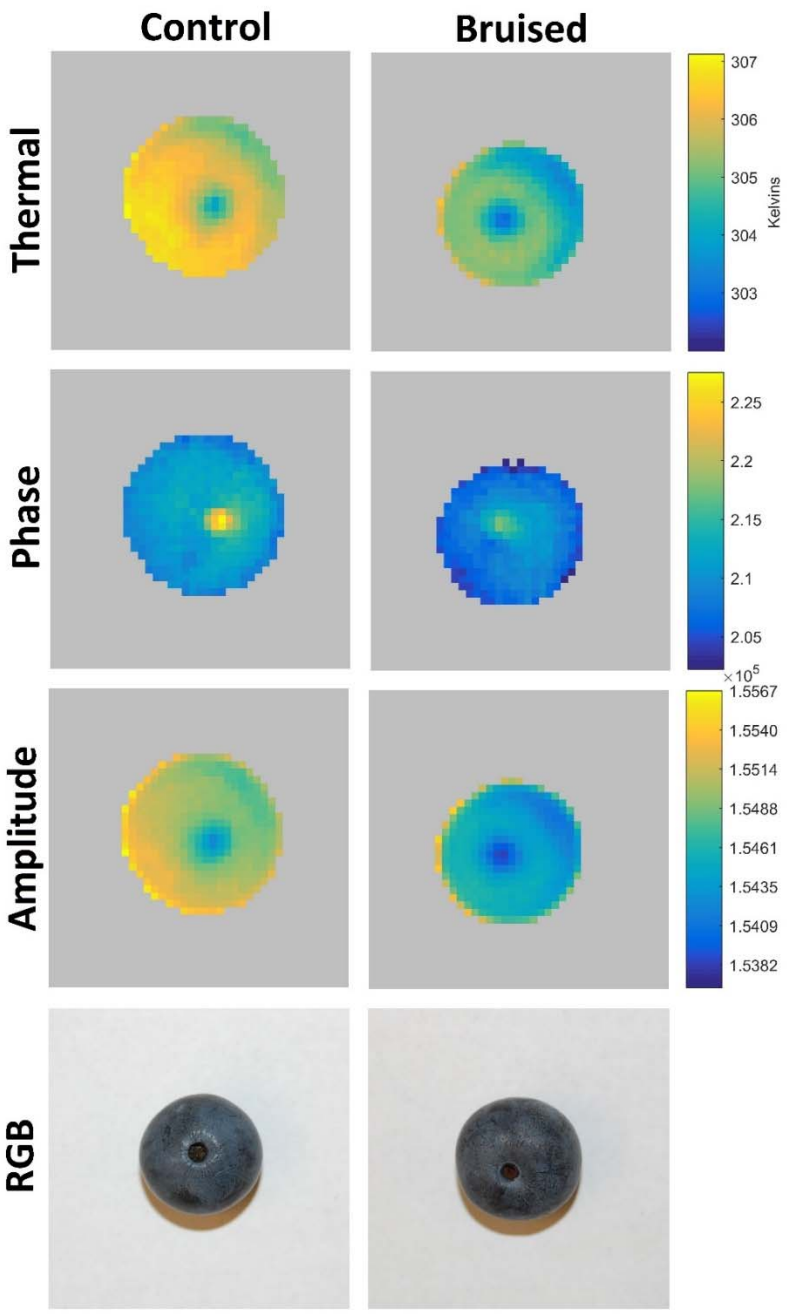

Figure 3.7. Thermal images, phasegrams, ampligrams and RBG images of healthy and bruised berries. Thermal color bar units are in Kelvins. Amplitude color bar units are unitless but roughly correspond to Kelvins. Phase color bar units are in radians.

ANOVA of the waveform features shows that calyx-end subsets are almost never statistically distinct, while stem-end subsets are consistently distinct on the rising and falling waveform features and peak temperature (Figures 3.8 and 3.9). Consequently, calyx-end data was excluded from further analysis. Unlike other features, the starting temperature feature did not show significant difference between control and bruised berries in both cultivars. These findings agree well with the previously-mentioned thermal window theory: bruised tissues have higher thermal diffusivity than control tissues. During the heating phase, received thermal radiation heats the surface of the berries. In both bruised and healthy berries, this heat energy is drawn from the exterior into the relatively cool interior by conduction. In the healthy berries, intact cell walls and organized cell layers impede this conduction (or thermal diffusion), while in bruised berries, ruptured cell walls and disrupted tissue layers with pockets of free water provide a better conductive medium. More of the heat on the surface of bruised tissues is therefore drawn from the exterior towards the interior, resulting in a lower surface temperature.

The indiscriminability of the calyx ends is best attributed to differences in the tissue types of the relevant physiological structures. Stem ends consist primarily of tissues consistent with the majority of the flesh of the fruit, with a relatively small pedicle. By contrast, calyxes consume much of the area of the calyx ends. Vestigial sepals obscure the underlying tissue with a differing thermal response due to their thin geometry, while the base of the calyx is noticeably stiff and woody compared to the remainder of the fruit tissue. This may result in less bruising in the calyx region when treated, smaller changes in thermal properties when bruising is present, or interference with examination of the underlying tissues.

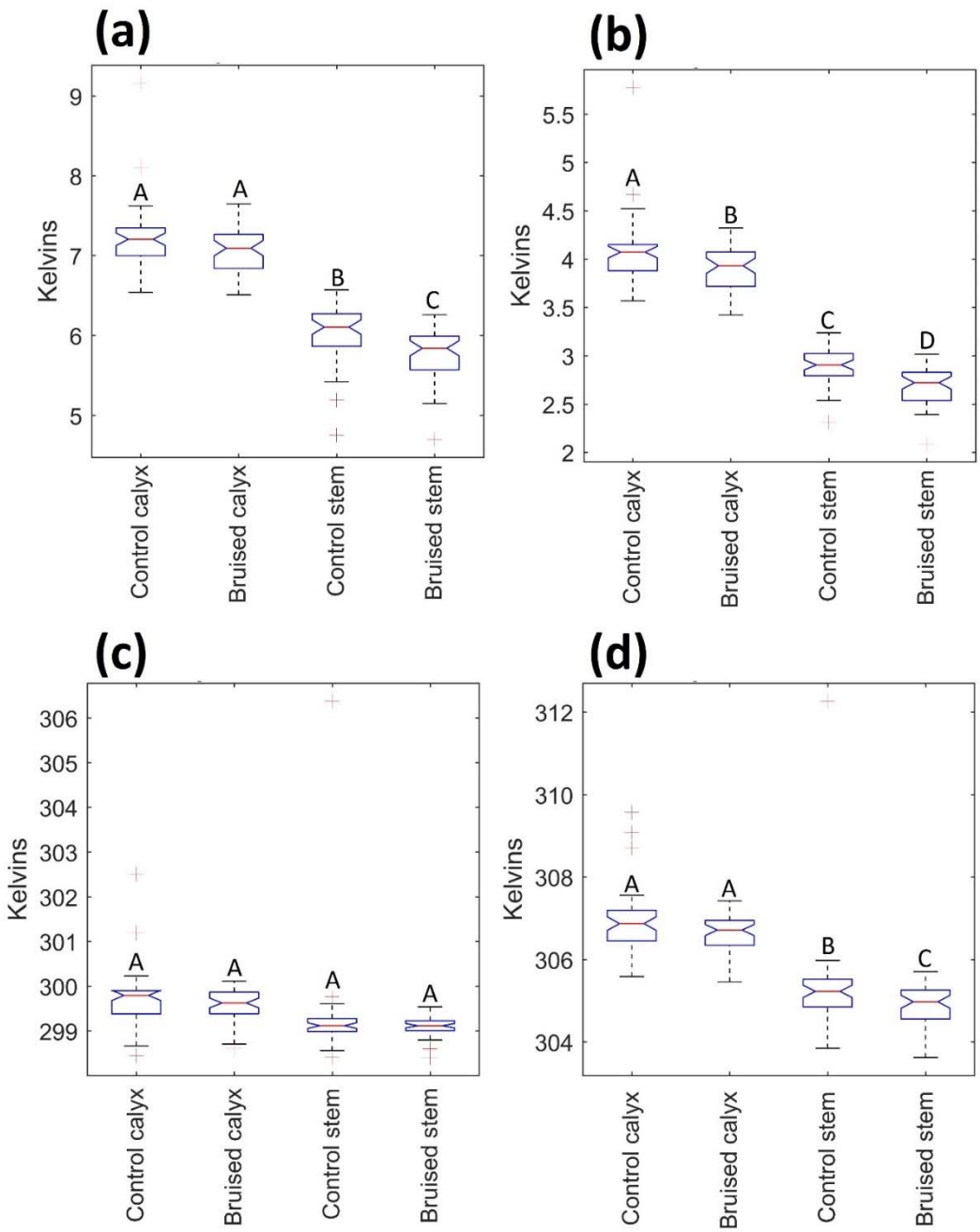

Figure 3.8. Box plots of waveform features, Farthing cultivar. (a) Rising waveform feature; (b) Falling waveform feature; (c) Starting temperatures; (d) Peak temperatures

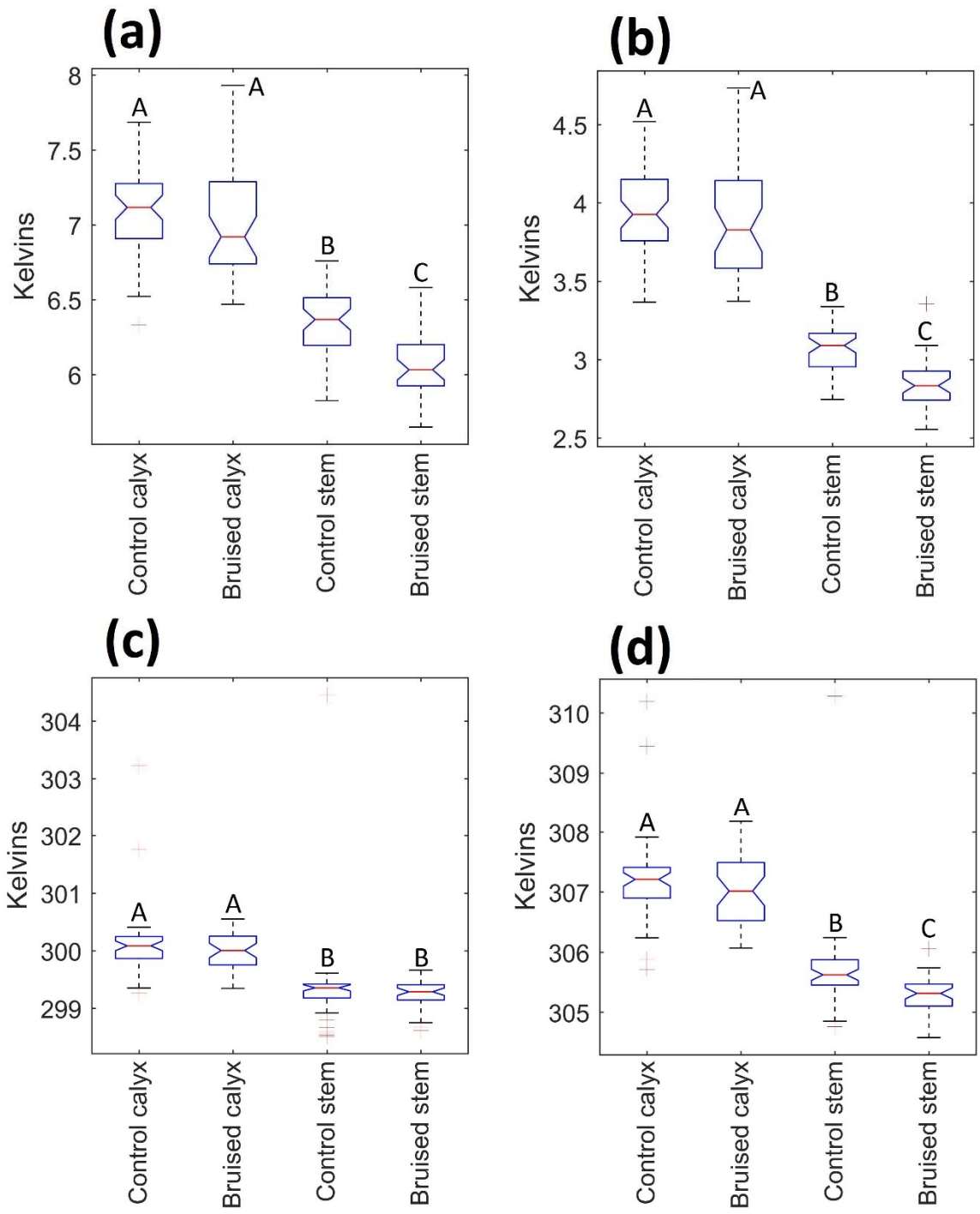

Figure 3.9. Box plots of waveform features, Meadowlark cultivar. (a) Rising waveform feature; (b) Falling waveform feature; (c) Starting temperatures; (d) Peak temperatures

3.3.4 Correlation between waveform features and bruise area index

Figures 3.10 and 3.11 show the results of linear correlation analysis of the bruise area index feature against the four waveform features for Farthing and Meadowlark subsets, respectively. Rising and falling waveform features and peak temperature all show strong statistical significance of correlation on both cultivars, with rising and falling waveform features being stronger than peak temperature. Starting temperature shows no statistical significance and weak r values, suggesting little relation between the amount of bruising and the starting temperature. The bruise area index was negatively correlated with the rising and falling waveform features, indicating that the less-bruised berries (control group) are more strongly affected by heating and cool more rapidly after heating. Likewise, healthier berries achieved a higher peak temperature than more-bruised berries. These findings are in alignment with the predictions of thermal window theory [5].

Overall, the two cultivars showed a similar pattern, although some differences between cultivars were observed. All correlations are more statistically significant for Farthing berries than for Meadowlark. This is perhaps related to the observed fact that many Meadowlark berries are less susceptible to bruising. Only very minor differences in the magnitude of the correlations were observed between cultivars.

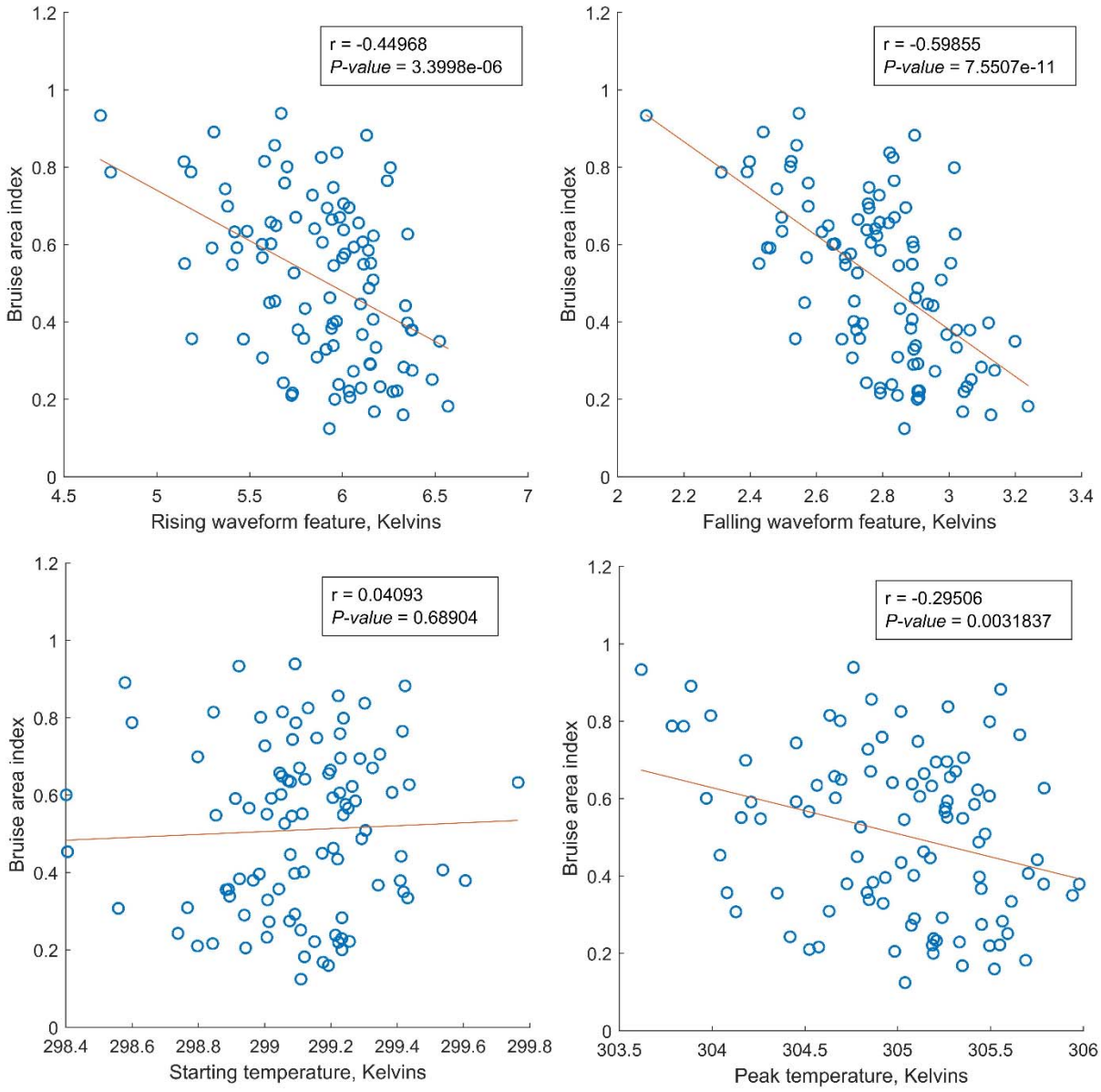

Figure 3.10. Correlation plots of bruise area index against waveform features, Farthing berries

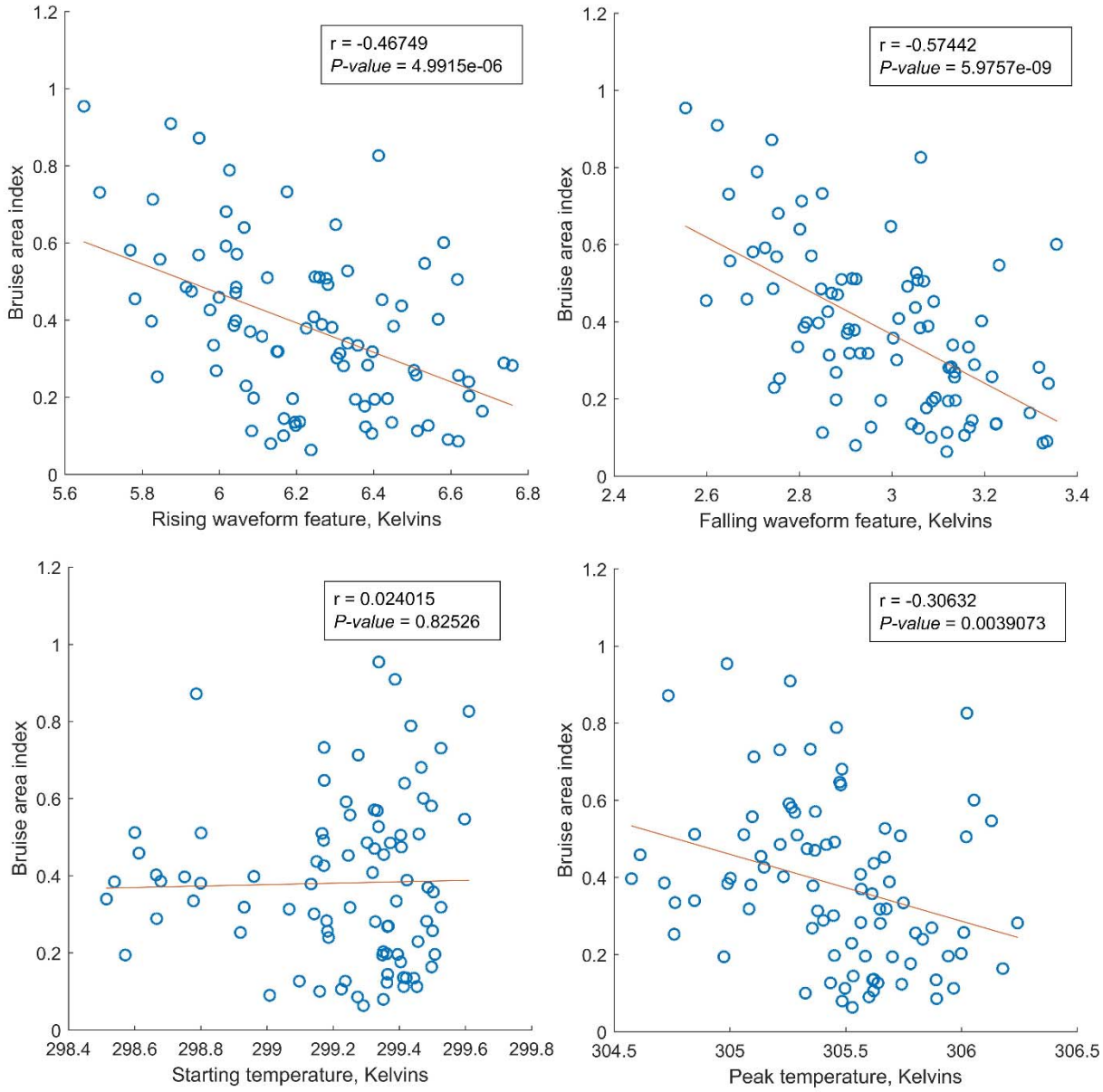

Figure 3.11. Correlation plots of bruise area index against waveform features, Meadowlark berries

3.3.5 MANOVA results and feature selection

MANOVA of feature sets showed strong statistical significance on all subsets (Table 3.1). The Farthing phase feature set was slightly weaker than the others, but was also strongly statistically significant. This indicates that all feature sets were suitable for use in classification

trials.

Table 3.1. P-values from MANOVA of feature sets on various data subsets

Feature set	Farthing	Meadowlark
Waveform	1.00E-04	1.00E-04
Whole amplitude	1.00E-04	1.00E-04
Whole phase	5.10E-03	1.00E-04

Examining the merit scores of the features (supplementary Table 3.4), it can be seen that the rising and falling waveform features were consistently the best performers, with the falling waveform feature being superior to the rising feature on all subsets. Mean amplitude features are next-best, followed by the waveform feature standard deviations. Phase features and amplitude standard deviation features were poor, and phase standard deviation features were very poor.

Based on the merit scores (Table 3.4 in Supplementary Materials), six additional feature sets were assembled for the purposes of classification. Feature set sizes were determined by selecting those features which returned merit scores on the full dataset equal to or greater than threshold values of 0.02 and 0.01, producing feature sets containing seven and thirteen features, respectively. A third feature set was assembled containing an empirically-selected set of the twenty highest-merit features on the full dataset. Having determined feature set sizes of seven, thirteen, and twenty features, feature sets were then extracted independently for each cultivar by taking the seven, thirteen, and twenty highest-merit features on each cultivar. These will be referred to as the "seven-feature sets," "thirteen-feature sets," and "twenty-feature sets," respectively.

3.3.6 Classification

The best classification accuracy obtained was 89.50% using waveform features, the Farthing

subset, and a logistic regression classifier. This trial also returned the highest kappa value of any trial, 0.79, indicating high reliability. The best classification accuracy for Meadowlark berries, 80.72%, was obtained with the twenty-feature set and the normalized linear kernel SVM, and had an associated kappa value of 0.61, indicating fair repeatability. Overall, waveform features out-performed amplitude and phase features.

Among the feature sets produced by feature selection, the general trend was improved accuracy in feature sets with a larger total number of features. Especially for the twenty-feature sets, accuracies tended to be on par with waveform feature set trials. If too many features were selected for these sets, it would be expected that cross-validated accuracies would decline due to overfitting as the number of features increased. The steadily increasing accuracies with increased feature numbers suggests that this threshold was not exceeded and that the feature sets are suitable for classification.

Farthing waveform results were highly dependent on the classifier used, while Meadowlark waveform results were more stable. No single best classifier is readily identified, although LDA and linear kernel normalized SVM are both strong performers. Normalization tended to improve the results of linear kernel SVM classifiers, while it significantly worsened many RBF kernel results. Linear kernel SVMs generally out-performed RBF-kernel SVMs, suggesting that the relationships between the features are relatively simple, that is, linear or near-linear, rather than multidimensional or interacting.

Regarding the disparity in classification accuracies between the cultivars, it is important to note that destructive evaluation showed significant heterogeneity of bruising in Meadowlark berries compared to Farthing berries, which by contrast tended to be thoroughly and uniformly bruised, and all of the samples which had to be removed due to insufficient bruising were

Meadowlark berries. This would seem to imply that Meadowlark berries are more resistant to bruising. If so, then the superior classification accuracy of Farthing berries over Meadowlark would most simply be attributed to more severe and complete bruising in the Farthing berries, and therefore larger changes in the thermal properties, leading to larger differences in the extracted waveform features.

Table 3.2. Table of classification accuracies, stem-end subsets

		SVM				Random Forest	LDA	Logistic Regression	K Nearest Neighbors
		Normalized		Non-normalized					
Cultivar	Feature set	RBF	Linear	RBF	Linear				
Farthing	Waveform	81.84	87.67	68.06	69.90	78.92	84.28	89.50	82.52
	Amplitude	67.69	82.57	51.09	81.99	77.60	82.57	79.90	73.73
	Phase	61.77	65.38	54.30	59.40	72.17	61.22	58.56	52.49
	7	67.99	66.49	46.47	68.18	72.13	72.18	71.58	66.21
	13	70.51	79.72	48.37	67.84	80.94	70.76	84.39	73.48
	20	74.99	83.34	54.59	84.06	81.01	82.58	78.53	67.39
Meadowlark	Waveform	78.63	76.39	77.71	78.63	74.94	76.26	77.89	73.72
	Amplitude	68.63	75.76	55.00	73.97	75.53	74.68	70.78	67.10
	Phase	53.53	74.11	58.39	65.11	78.06	73.99	70.11	62.14
	7	76.94	76.01	61.57	75.56	73.89	77.26	76.93	69.28
	13	78.61	79.06	55.00	74.46	78.99	77.74	76.76	72.56
	20	79.74	80.72	55.00	75.36	78.85	77.67	75.43	73.43

3.4 CONCLUSION

Significant differences between bruised and healthy berries were present only between stem ends, with virtually no significant differences between calyx ends. Among stem-end subsets, healthy berries displayed more rapid surface temperature fluctuations during both the heating and

cooling phases, which is supported by the thermal window theory. Good classification accuracies were produced from the waveform feature set and the twenty-feature selected sets including amplitude and phase features in the frequency domain, yielding top accuracies of 90% and 80% for Farthing and Meadowlark cultivars, respectively. The results presented here suffice as a proof of concept that pulsed thermographic imaging could be used to detect blueberry internal bruising due to differences in thermal properties between healthy and bruised tissues. The thermal imaging technique could be considered as one viable sensing technique given the large temperature fluctuation blueberries experience in postharvest handling.

Acknowledgments

This work was supported by the National Institute for Food and Agriculture [grant number: 2014-51181-22383].

3.5 REFERENCES

1. Yu, P.; Li, C.; Takeda, F.; Krewer, G.; Rains, G.; Hamrita, T. Measurement of mechanical impacts created by rotary, slapper, and sway blueberry mechanical harvesters. *Computers and electronics in agriculture* **2014**, *101*, 84-92.
2. Tritz, J.M. System and method for automated tactile sorting. Google Patents: 2013.
3. Maldague, X. Theory and practice of infrared technology for nondestructive testing. **2001**.
4. Danno, A.; Miyazato, M.; Ishiguro, E. Quality evaluation of agricultural products by infrared imaging method. *Memoirs Fac Agric* **1978**, *14*, 123-138.

5. Varith, J.; Hyde, G.; Baritelle, A.; Fellman, J.; Sattabongkot, T. Non-contact bruise detection in apples by thermal imaging. *Innovative Food Science & Emerging Technologies* **2003**, *4*, 211-218.

6. Baranowski, P.; Mazurek, W.; Witkowska-Walczak, B.; Sławiński, C. Detection of early apple bruises using pulsed-phase thermography. *Postharvest biology and technology* **2009**, *53*, 91-100.

7. Baranowski, P.; Mazurek, W.; Wozniak, J.; Majewska, U. Detection of early bruises in apples using hyperspectral data and thermal imaging. *Journal of Food Engineering* **2012**, *110*, 345-355.

8. Kim, G.; Kim, G.-H.; Park, J.; Kim, D.-Y.; Cho, B.-K. Application of infrared lock-in thermography for the quantitative evaluation of bruises on pears. *Infrared Physics & Technology* **2014**, *63*, 133-139.

9. Kuzy, J.; Li, C. A pulsed thermographic imaging system for detection and identification of cotton foreign matter. *Sensors* **2017**, *17*, 518.

10. Baranowski, P.; Lipecki, J.; Mazurek, W.; Walczak, R.T. Detection of watercore in 'gloster'apples using thermography. *Postharvest biology and technology* **2008**, *47*, 358-366.

11. Ginesu, G.; Giusto, D.D.; Märgner, V.; Meinlschmidt, P. Detection of foreign bodies in food by thermal image processing. *Industrial Electronics, IEEE Transactions on* **2004**, *51*, 480-490.

12. Gowen, A.; Tiwari, B.; Cullen, P.; McDonnell, K.; O'Donnell, C. Applications of thermal imaging in food quality and safety assessment. *Trends in food science & technology* **2010**, *21*, 190-200.

13. Hellebrand, H.; Herppich, W.; Beuche, H.; Dammer, K.; Linke, M.; Flath, K. Investigations of plant infections by thermal vision and nir imaging. *International agrophysics* **2006**, *20*, 1.

14. Ishikawa, M.; Hatta, H.; Habuka, Y.; Fukui, R.; Utsunomiya, S. Detecting deeper defects using pulse phase thermography. *Infrared Physics & Technology* **2013**, *57*, 42-49.

15. Maldague, X.; Marinetti, S. Pulse phase infrared thermography. *Journal of Applied Physics* **1996**, *79*, 2694-2698.

16. Maldague, X.; Galmiche, F.; Ziadi, A. Advances in pulsed phase thermography. *Infrared physics & technology* **2002**, *43*, 175-181.

17. Maldague, X.; Largouët, Y.; Couturier, J.-P. A study of defect depth using neural networks in pulsed phase thermography: Modelling, noise, experiments. *Revue Générale de Thermique* **1998**, *37*, 704-717.

18. Offermann, S.; Bicanic, D.; Claude Krapez, J.; Balageas, D.; Gerkema, E.; Chirtoc, M.; Egee, M.; Keijzer, K.; Jalink, H. Infrared transient thermography for non-contact, nondestructive inspection of whole and dissected apples and of cherry tomatoes at different maturity stages. *Instrumentation science & technology* **1998**, *26*, 145-155.

19. Vavilov, V.; Marinetti, S. Pulsed phase thermography and fourier-analysis thermal tomography. *Russian journal of nondestructive testing* **1999**, *35*, 134-145.

20. Vadivambal, R.; Jayas, D. Applications of thermal imaging in agriculture and food industry—a review. *Food Bioprocess Technol* **2011**, *4*, 186-199.

21. Warmann, C.; Märgner, V. In *Quality control of hazel nuts using thermographic image processing*, MVA, 2005; pp 84-87.

22. Veraverbeke, E.A.; Verboven, P.; Lammertyn, J.; Cronje, P.; De Baerdemaeker, J.; Nicolaï, B.M. Thermographic surface quality evaluation of apple. *Journal of Food Engineering* **2006**, *77*, 162-168.

3.6 SUPPLEMENTARY MATERIALS

Table 3.3. Independent and interactance p-values for treatment, orientation, and cultivar from ANOVA of rising waveform feature

Feature(s)	P-value
Treatment	<.0001
Orientation	<.0001
Cultivar	0.0002
Treatment * Orientation	0.0123
Treatment * Cultivar	0.7615
Orientation * Cultivar	<.0001
Treatment * Orientation * Cultivar	0.523

Table 3.4. Results of RELIEFF feature evaluation

	Dataset					
	Farthing		Meadowlark		Average	
Feature	Merit	Rank	Merit	Rank	Merit	Rank
rising waveform	0.050	2.5	0.075	2.2	0.063	2.350
falling waveform	0.056	1.0	0.089	1.0	0.073	1.000
rising waveform std	0.005	19.9	0.007	21.5	0.006	20.700
falling waveform std	0.013	11.1	0.005	26.4	0.009	18.750
whole amp 1	0.023	7.0	0.018	9.8	0.021	8.400
whole amp 2	0.041	4.0	0.072	2.8	0.057	3.400
whole amp 3	0.049	2.5	0.041	4.6	0.045	3.550
whole amp 4	0.020	7.1	0.016	10.5	0.018	8.800
whole amp 5	0.015	9.2	0.008	20.5	0.012	14.850
whole amp 6	0.014	10.2	0.026	7.1	0.020	8.650
whole amp 7	0.010	13.0	0.017	10.2	0.014	11.600
whole amp 8	0.004	23.8	0.001	34.7	0.003	29.250

whole amp 9	0.010	13.4	0.017	10.2	0.014	11.800
whole amp 10	0.001	31.3	-0.007	44.8	-0.003	38.050
whole amp std 1	0.003	26.4	0.004	26.7	0.004	26.550
whole amp std 2	0.007	16.2	0.005	27.0	0.006	21.600
whole amp std 3	0.004	22.5	0.004	28.9	0.004	25.700
whole amp std 4	0.004	23.5	0.009	17.5	0.007	20.500
whole amp std 5	0.002	28.4	0.010	17.0	0.006	22.700
whole amp std 6	0.004	24.0	0.006	22.2	0.005	23.100
whole amp std 7	0.003	26.4	0.004	29.2	0.004	27.800
whole amp std 8	0.001	32.9	0.010	17.5	0.006	25.200
whole amp std 9	0.002	29.6	0.004	26.6	0.003	28.100
whole amp std 10	-0.001	37.8	0.005	24.8	0.002	31.300
whole phase 1	0.021	7.0	0.040	4.4	0.031	5.700
whole phase 2	0.009	14.0	0.000	38.9	0.005	26.450
whole phase 3	-0.017	46.0	0.003	31.0	-0.007	38.500
whole phase 4	0.016	8.5	0.012	14.5	0.014	11.500
whole phase 5	-0.002	39.9	0.008	21.3	0.003	30.600
whole phase 6	0.005	22.8	0.005	26.5	0.005	24.650
whole phase 7	0.004	22.3	0.001	37.1	0.003	29.700
whole phase 8	0.005	23.7	-0.003	42.9	0.001	33.300
whole phase 9	0.005	21.7	-0.011	45.5	-0.003	33.600
whole phase 10	-0.001	36.5	0.009	19.6	0.004	28.050
whole phase std 1	0.005	21.4	0.029	6.7	0.017	14.050
whole phase std 2	0.006	21.4	0.001	35.0	0.004	28.200
whole phase std 3	-0.006	44.5	0.008	19.8	0.001	32.150
whole phase std 4	-0.005	43.4	0.003	31.3	-0.001	37.350
whole phase std 5	0.001	32.8	0.012	14.8	0.007	23.800
whole phase std 6	0.002	29.3	0.005	24.0	0.004	26.650
whole phase std 7	-0.001	37.7	0.001	38.0	0.000	37.850
whole phase std 8	-0.003	41.5	-0.003	43.5	-0.003	42.500
whole phase std 9	-0.002	40.1	0.001	36.5	-0.001	38.300
whole phase std 10	-0.001	38.7	0.004	28.2	0.002	33.450

Table 3.5. Cohen's Kappa for classification trials

Cultivar	Feature set	Classifier							
		SVM							
		Normalized		Non-normalized					
		RBF	Linear	RBF	Linear	Random Forest	LDA	Logistic Regression	K Nearest Neighbors
Farthing	Waveform	0.64	0.75	0.36	0.40	0.58	0.69	0.79	0.65
	Amplitude	0.36	0.65	0.04	0.64	0.55	0.65	0.60	0.47
	Phase	0.24	0.31	0.09	0.19	0.44	0.22	0.17	0.05
	7	0.36	0.33	-0.05	0.36	0.46	0.44	0.43	0.33
	13	0.41	0.60	-0.01	0.37	0.61	0.41	0.69	0.47
	20	0.47	0.72	0.11	0.67	0.65	0.63	0.54	0.40
Meadowlark	Waveform	0.56	0.52	0.54	0.56	0.49	0.52	0.55	0.46
	Amplitude	0.33	0.51	0.00	0.48	0.50	0.48	0.41	0.32
	Phase	-0.03	0.45	0.09	0.25	0.55	0.47	0.40	0.23
	7	0.53	0.51	0.18	0.51	0.49	0.54	0.53	0.38
	13	0.56	0.57	0.00	0.47	0.58	0.55	0.53	0.44
	20	0.58	0.61	0.00	0.50	0.59	0.55	0.51	0.46

CHAPTER 4

CONCLUSION

Both tasks attempted were performed with some success. As predicted, cotton trash detection was the easier of the two; differences of up to forty degrees Celsius between the peak temperatures achieved by different foreign matter types rendered some portions of identification trivially easy. Moreover, the separability of cotton from most debris types on at least one of the derived features enables a near-perfect discrimination between cotton and all types of foreign matter. Further, the ability to distinguish between foreign matter types is of significant utility, as this can provide the basis for foreign matter scoring which is more sensitive to the nature of the debris present, potentially enabling a more discriminating allocation of various grades of cotton to different uses.

One issue that remains to be investigated is the penetrability of the technique; the feasibility of detecting and identifying foreign matter that is not on the surface of the cotton lint, but inside of it, partially or wholly obscured from view. Absent the ability to reveal such foreign matter, the technique will only provide a sampling of the foreign matter present, rather than a comprehensive inventory. This is still an improvement on visual grading, which is of course likewise non-penetrating, but is nonetheless a shortcoming.

Another shortcoming of the study is the relative uniformity of shape and large size of the foreign matter samples used. Most foreign matter that is present following ginning has been reduced to minute fragments, which may prove significantly more difficult to detect. However, a

sufficient image resolution of the detecting system should ameliorate most of the issues that this would entail.

Blueberry bruise detection was more difficult and results were more mixed. Unlike the fruit bruise detection studies performed by previous researchers, visualization of the bruises was not possible. This is likely due to a number of factors, all of which, in sum, amount to the significant physiological differences between blueberries and the fruits used in previous studies. The tissues of apples and pears are less dense than water, whereas those of blueberries are more dense. Apples and pears are much firmer than blueberries. Lastly, the relatively large size of apples and pears makes the discrimination of a relatively small bruise on their surfaces easier; curvature effects and edge effects are of less concern. Nonetheless, certain combinations of feature sets and classifiers achieved respectable accuracies of discrimination. On the other hand, the use of an extreme bruising treatment, producing berries which were certainly so badly bruised as to be screened out by a soft-sorting device, raises the question of whether a good accuracy can be had in detecting more moderate bruises. As the results stand, this study can serve, at a minimum, as a proof of concept that bruising results in differences in the material properties of blueberries which can, in turn, be detected by pulsed thermographic analysis. Additional studies with more moderate treatments, attempting, perhaps, to discriminate between bruises of varying severity, can now be performed on the basis of these findings.

Pulsed thermographic inspection is a powerful tool for the evaluation of post-harvest quality for a variety of crops. Whenever the discrimination that is desired is to be made on the basis of materials that differ significantly in their material properties, there is an opportunity to detect these differences by thermographic examination. In this thesis, the potential for applying this technique to the problems of cotton foreign matter detection and blueberry bruise detection

has been shown to be feasible, and in the case of cotton foreign matter detection, perhaps even extraordinarily efficacious. With further study, these techniques may someday find industrial application; for the time being, a theoretical basis has been established for their application, paving the way for fine-grained investigation of further problems in the domain.

REFERENCES

1. Himmelsbach, D.S.; Hellgeth, J.W.; McAlister, D.D. Development and use of an attenuated total reflectance/fourier transform infrared (atr/ft-ir) spectral database to identify foreign matter in cotton. *Journal of agricultural and food chemistry* **2006**, *54*, 7405-7412.
2. Federation, I.T.M. Itmf cotton contamination survey. Zurich, Switzerland, 2014.
3. Ghorashi, H. Uster® hvi classic. Technologies, U., Ed. CI Singapore, 2004.
4. Xu, B.; Fang, C.; Huang, R.; Watson, M.D. Chromatic image analysis for cotton trash and color measurements. *Textile research journal* **1997**, *67*, 881-890.
5. Yang, W.; Li, D.; Wei, X.; Kang, Y.; Li, F. In *An automated visual inspection system for foreign fiber detection in lint*, 2009 WRI Global Congress on Intelligent Systems, 2009; IEEE: pp 364-368.
6. Fortier, C.A.; Rodgers, J.E.; Cintron, M.S.; Cui, X.; Foulk, J.A. Identification of cotton and cotton trash components by fourier transform near-infrared spectroscopy. *Textile Research Journal* **2011**, *81*, 230-238.
7. Fortier, C.; Rodgers, J.; Foulk, J.; Whitelock, D. Near-infrared classification of cotton lint, botanical and field trash. *Journal of cotton science* **2012**.

8. Guo, J.; Ying, Y.; Li, J.; Rao, X.; Kang, Y.; Shi, Z. Detection of foreign materials on surface of ginned cotton by hyper-spectral imaging. *Transactions of the Chinese society of agricultural engineering* **2012**, *28*, 126-134.

9. Zhang, R.; Li, C.; Zhang, M.; Rodgers, J. Shortwave infrared hyperspectral reflectance imaging for cotton foreign matter classification. *Computers and Electronics in Agriculture* **2016**, *127*, 260-270.

10. Gamble, G.R.; Foulk, J.A. Quantitative analysis of cotton (gossypium hirsutum) lint trash by fluorescence spectroscopy. *Journal of agricultural and food chemistry* **2007**, *55*, 4940-4943.

11. Mustafic, A.; Li, C. Classification of cotton foreign matter using color features extracted from fluorescent images. *Textile Research Journal* **2015**, *85*, 1209-1220.

12. Pai, A.S. X-ray microtomographic image analysis for identification of cotton contaminants. Texas Tech University, 2002.

13. Pai, A.; Sari-Sarraf, H.; Hequet, E.F. Recognition of cotton contaminants via x-ray microtomographic image analysis. *IEEE Transactions on Industry Applications* **2004**, *40*, 77-85.

14. Meinlschmidt, P.; Maergner, V. In *Detection of foreign substances in food using thermography*, AeroSense 2002, 2002; International Society for Optics and Photonics: pp 565-571.

15. Matiacevich, S.; Cofr, C.; #xe9; , D.; Silva, P.; Enrione, J.; Osorio, F. Quality parameters of six cultivars of blueberry using computer vision. *International Journal of Food Science* **2013**, *2013*, 8.

16. MatIaCeVIC, S.; SILV, P. Evaluation of blueberry color during storage by image analysis. *Color in Food: Technological and Psychophysical Aspects* **2012**, 211.

17. Leiva-Valenzuela, G.A.; Aguilera, J.M. Automatic detection of orientation and diseases in blueberries using image analysis to improve their postharvest storage quality. *Food Control* **2013**, *33*, 166-173.

18. Leiva-Valenzuela, G.A.; Lu, R.; Aguilera, J.M. Prediction of firmness and soluble solids content of blueberries using hyperspectral reflectance imaging. *Journal of Food Engineering* **2013**, *115*, 91-98.

19. Jiang, Y.; Li, C.; Takeda, F. Nondestructive detection and quantification of blueberry bruising using near-infrared (nir) hyperspectral reflectance imaging. *Scientific Reports* **2016**, *6*, 35679.

20. Leiva-Valenzuela, G.A.; Lu, R.; Aguilera, J.M. Assessment of internal quality of blueberries using hyperspectral transmittance and reflectance images with whole spectra or selected wavelengths. *Innovative Food Science & Emerging Technologies* **2014**, *24*, 2-13.

21. Hu, M.-H.; Dong, Q.-L.; Liu, B.-L.; Opara, U.L. Prediction of mechanical properties of blueberry using hyperspectral interactance imaging. *Postharvest Biology and Technology* **2016**, *115*, 122-131.

22. Li, C.; Krewer, G.W.; Ji, P.; Scherm, H.; Kays, S.J. Gas sensor array for blueberry fruit disease detection and classification. *Postharvest Biology and Technology* **2010**, *55*, 144-149.

23. Demir, N.; Ferraz, A.C.O.; Sargent, S.A.; Balaban, M.O. Classification of impacted blueberries during storage using an electronic nose. *Journal of the Science of Food and Agriculture* **2011**, *91*, 1722-1727.

24. Danno, A.; Miyazato, M.; Ishiguro, E. Quality evaluation of agricultural products by infrared imaging method. *Memoirs Fac Agric* **1978**, *14*, 123-138.

25. Baranowski, P.; Mazurek, W.; Witkowska-Walczak, B.; Sławiński, C. Detection of early apple bruises using pulsed-phase thermography. *Postharvest biology and technology* **2009**, *53*, 91-100.

26. Baranowski, P.; Mazurek, W.; Wozniak, J.; Majewska, U. Detection of early bruises in apples using hyperspectral data and thermal imaging. *Journal of Food Engineering* **2012**, *110*, 345-355.

27. Varith, J.; Hyde, G.; Baritelle, A.; Fellman, J.; Sattabongkot, T. Non-contact bruise detection in apples by thermal imaging. *Innovative Food Science & Emerging Technologies* **2003**, *4*, 211-218.

28. Kim, G.; Kim, G.-H.; Park, J.; Kim, D.-Y.; Cho, B.-K. Application of infrared lock-in thermography for the quantitative evaluation of bruises on pears. *Infrared Physics & Technology* **2014**, *63*, 133-139.

29. Frater, M.R.; Arnold, J.F. Coding of 12-bit video from thermal imaging systems. *Signal Processing: Image Communication* **2000**, *15*, 907-916.

30. Mc Cullagh, J.; Setchell, D.; Gulabivala, K.; Hussey, D.; Biagioni, P.; Lamey, P.J.; Bailey, G. A comparison of thermocouple and infrared thermographic analysis of temperature rise on the root surface during the continuous wave of condensation technique. *International Endodontic Journal* **2000**, *33*, 326-332.

31. Shepard, S.M.; Ahmed, T.; Lhota, J.R. In *Experimental considerations in vibrothermography*, Defense and Security, 2004; International Society for Optics and Photonics: pp 332-335.

32. Maldague, X.; Ziadi, A.; Klein, M. Double pulse infrared thermography. *NDT E Int.* **2004**, *37*, 559-564.

33. Maldague, X.; Marinetti, S. Pulse phase infrared thermography. *Journal of Applied Physics* **1996**, *79*, 2694-2698.

34. Ibarra-Castanedo, C.; Maldague, X. In *Review of pulse phase thermography*, SPIE Sensing Technology+ Applications, 2015; International Society for Optics and Photonics: pp 94850T-94850T-94810.